Photosynthesis Research
https://doi.org/10.1007/s11120-019-00621-0

ORIGINAL ARTICLE

The Antarctic psychrophiles *Chlamydomonas* spp. UWO241 and ICE-MDV exhibit differential restructuring of photosystem I in response to iron

Greg Cook[1] · Amber Teufel[1] · Isha Kalra[1] · Wei Li[2] · Xin Wang[1] · John Priscu[2] · Rachael Morgan-Kiss[1]

Received: 17 July 2018 / Accepted: 25 January 2019

Abstract

Chlamydomonas sp. UWO241 is a psychrophilic alga isolated from the deep photic zone of a perennially ice-covered Antarctic lake (east lobe Lake Bonney, ELB). Past studies have shown that *C.* sp. UWO241 exhibits constitutive downregulation of photosystem I (PSI) and high rates of PSI-associated cyclic electron flow (CEF). Iron levels in ELB are in the nanomolar range leading us to hypothesize that the unusual PSI phenotype of *C.* sp. UWO241 could be a response to chronic Fe-deficiency. We studied the impact of Fe availability in *C.* sp. UWO241, a mesophile, *C. reinhardtii* SAG11-32c, as well as a psychrophile isolated from the shallow photic zone of ELB, *Chlamydomonas* sp. ICE-MDV. Under Fe-deficiency, PsaA abundance and levels of photooxidizable P700 ($\Delta A_{820}/A_{820}$) were reduced in both psychrophiles relative to the mesophile. Upon increasing Fe, *C.* sp. ICE-MDV and *C. reinhardtii* exhibited restoration of PSI function, while *C.* sp. UWO241 exhibited only moderate changes in PSI activity and lacked almost all LHCI proteins. Relative to Fe-excess conditions (200 µM Fe^{2+}), *C.* sp. UWO241 grown in 18 µM Fe^{2+} exhibited downregulation of light harvesting and photosystem core proteins, as well as upregulation of a bestrophin-like anion channel protein and two CEF-associated proteins (NdsS, PGL1). Key enzymes of starch synthesis and shikimate biosynthesis were also upregulated. We conclude that in response to variable Fe availability, the psychrophile *C.* sp. UWO241 exhibits physiological plasticity which includes restructuring of the photochemical apparatus, increased PSI-associated CEF, and shifts in downstream carbon metabolism toward storage carbon and secondary stress metabolites.

Keywords Antarctica · Cyclic electron flow · Iron · Photosystem I · Psychrophile

Abbreviations

$\Delta\psi$	Electric field gradient
A_{820}	P700 + absorbance at 820 nm
Δ/A_{820}	Proportion of photooxidizable P700
AL	Actinic light
CEF	Cyclic electron flow
Chl a	Chlorophyll *a*
e^-/P700	Intersystem electron pool size per PSI reaction center
ELB	East lobe Lake Bonney
F_{685}	77 K fluorescence maximum, 685 nm
F_{715}	77 K fluorescence maximum, 715 nm
FR	Far red
F_V/F_M	Maximum photosynthetic efficiency
HNLC	High nutrient, low chlorophyll
LHCI	Light harvesting complex I
LHCII	Light harvesting complex II
MT/ST	Multiple turn-over/single turn-over actinic light flash
NPQ	Nonphotochemical quenching
P700+	Photochemical reaction center of photosystem I, oxidized form
pmf	Proton motive force
PSI	Photosystem I
PSII	Photosystem II
qP	Photochemical quenching

Electronic supplementary material The online version of this article (https://doi.org/10.1007/s11120-019-00621-0) contains supplementary material, which is available to authorized users.

✉ Rachael Morgan-Kiss
morganr2@miamioh.edu

[1] Department of Microbiology, Miami University, 700 E High St., 32 Pearson Hall, Oxford, OH 45056, USA

[2] Land Resources and Environmental Sciences, Montana State University, Bozeman, MT, USA

Published online: 07 February 2019

$t_{1/2}^{red}$	Half-time for re-reduction of P700+
Y(PSI)	Effective quantum yield of PSI
Y(PSII)	Effective quantum yield of PSII
Y(NA)	Energy loss due to acceptor side limitation
Y(ND)	Energy loss due to donor side limitation
Y(NO)	Energy dissipation from nonregulated processes
Y(NPQ)	Nonphotochemical energy dissipation from antenna quenching

Introduction

Iron, one of the most abundant elements on Earth, resides in multiple forms in aquatic environments, including solutions or colloids. The soluble, bioavailable form of iron, ferrous (Fe^{2+}), is often below biological needs in aquatic environments (Martin and Fitzwater 1988). Although essential for multiple metabolic pathways involving redox reactions, iron is particularly important for several photosynthetic activities and therefore has important implications on global primary production. Almost 50% of primary production occurs in oceans which contain sub-nanomolar Fe concentrations, i.e., much of the carbon fixation in aquatic habitats occurs under Fe-limiting conditions (Bowie et al. 2002; Behrenfeld and Kolber 1999; Coale et al. 2004). The "iron hypothesis" predicts that over large geological time scales iron supply played a critical role in oscillations in atmospheric CO_2 concentrations and climate through control of ocean phytoplankton productivity (Martin 1990).

The photosynthetic electron transport chain is enriched in iron. Fe-limitation specifically targets photosystem I (PSI) as it requires three 4Fe–4S centers (i.e., 12 atoms of Fe per complex) as electron acceptors and contains almost half of the iron content present within the photosynthetic apparatus (Merchant et al. 2006). The Cyt b_6f complex also has relatively high Fe needs (6 atoms per complex), while PSII requires only two Fe atoms per complex. Ratios of PSI/PSII are significantly reduced in cyanobacteria and algae acclimated to Fe-limiting conditions (Straus 1994; Strzepek and Harrison 2004; Moseley et al. 2002; Ivanov et al. 2000; Glaesener et al. 2013). Moreover, deficiencies on the electron acceptor side of PSI lead to rapid over-reduction of PSI photochemistry and generation of the reactive oxygen species, superoxide (Spreitzer and Mets 1981; Sonoike and Terashima 1994; Sonoike et al. 1995). As PSI lacks an efficient repair cycle, photoprotection of PSI is important under Fe-limitation. This is accomplished in part by downregulation of PSI through uncoupling of light harvesting complex I (LHCI) from PSI (Desquilbet et al. 2003; Merchant et al. 2006) (i.e., functional downregulation), as well as degradation of specific LHCI subunits (i.e., structural downregulation) (Naumann et al. 2005, 2007) in plants and algae. Major remodeling of LHCI-PSI as well as accumulation of novel PSI antenna proteins has been observed in cyanobacteria (Bibby et al. 2001) and algae (Yadavalli et al. 2012; Varsano et al. 2006). LHCI-PSI downregulation can be monitored as a reduction in PSI-associated low temperature (77 K) Chl *a* fluorescence emission peak at 715–720 nm (Yadavalli et al. 2012). Iron deficiency also results in a reduction in the level of photooxidizable P700 and faster rates of P700+ re-reduction (Elkhouni et al. 2018; Ivanov et al. 2012).

A large proportion (up to 70%) of the Earth's habitable space is permanently or seasonally cold (< 5 °C) (e.g., world's oceans, polar regions, alpine habitats) (De Maayer et al. 2014). Where there is light and low temperature, food webs are supported by the "photopsychrophiles", representing cold-adapted cyanobacteria, photosynthetic bacteria, and algae (Morgan-Kiss et al. 2006; Cvetkovska et al. 2017). Photopsychrophiles employ novel strategies to balance energy flow between processes which are largely temperature-insensitive (i.e., light absorption, energy transduction) and downstream metabolic pathways which are highly sensitive to the external thermal environment. Last, cold adapted photosynthetic microorganisms must survive permanent low temperatures combined with other stresses (nutrient stress, hypersalinity, high UV, desiccation), including nanomolar concentrations of bioavailable iron in the Antarctic (De Baar et al. 1995) and northeast Pacific subarctic oceans (Martin and Fitzwater 1988). While there have been numerous studies on the effect of Fe-availability on polar phytoplankton productivity (Boyd et al. 2000; Martin and Fitzwater 1988; Coale et al. 2004), a thorough understanding of the additive effects of photosynthetic adaptation to low temperatures combined with chronic Fe-deficiency is currently lacking.

The McMurdo (MCM) Dry Valleys (southern Victoria Land, Antarctica) are a polar desert with annual temperatures averaging − 20 °C and annual precipitation < 10 cm (Lyons et al. 2000). Despite these extreme conditions, microbial-dominated food webs persist in water columns of numerous ice-covered lakes and ponds (Morgan-Kiss et al. 2006; Priscu et al. 1999). The Antarctic psychrophile, *Chlamydomonas* sp. UWO241 was isolated from the deep photic zone (17 m depth) of east lobe Lake Bonney (ELB), one of several highly studied MCM lakes. Due to the unusual physicochemistry of the ELB water column, *C.* sp. UWO241 is adapted to low temperatures, hypersalinity and extreme shade of unusual spectral quality (blue wavelengths) (Neale and Priscu 1995). The permanent ice-cover prevents vertical mixing: phytoplankton communities of variable composition are layered within a highly stratified photic zone characterized by freshwater/oligotrophic conditions at the surface and hypersaline/mesotrophic in the deeper layers (Bielewicz et al. 2011). Early studies showed that ELB phytoplankton are extremely phosphorus deficient (Priscu 1995; Dore and Priscu 2001; Teufel et al. 2017). Micronutrients were not investigated in these

studies, but iron is low or below detection limits within the photic zone of ELB (Weand et al. 1976; Ward et al. 2003; Angino et al. 1964).

Past studies have described in detail how the photosynthetic apparatus of *C*. sp. UWO241 is restructured compared with other mesophilic model algae to survive conditions of constitutive long-term stress (Morgan et al. 1998; Morgan-Kiss et al. 2002a, b, 2005; Szyszka et al. 2007). One of the more intriguing characteristics of *C*. sp. UWO241 is an apparent permanent downregulation of PSI, estimated by the absence of a measurable PSI-associated low temperature (77 K) Chl *a* fluorescence emission peak (Morgan et al. 1998) combined with low levels of photooxidizable P700 ($\Delta A_{820}/A_{820}$), and an apparent absence of all or most LHCI proteins (Morgan et al. 1998; Morgan-Kiss et al. 2002b; Szyszka-Mroz et al. 2015). In addition, *C*. sp. UWO241 maintains constitutively high rates of PSI-associated cyclic electron flow (CEF) rates which are associated with formation of a stable PSI supercomplex (Morgan-Kiss et al. 2005; Szyszka et al. 2007; Szyszka-Mroz et al. 2015). The unusual characteristic of an apparent downregulation of PSI in *C*. sp. UWO241 resembles an Fe-deficient phenotype in other algae grown under laboratory-controlled conditions (Merchant et al. 2006; Yadavalli et al. 2012). As a strategy for survival under long-term Fe-limitation, natural communities of oceanic diatoms reduce their cellular Fe requirements relative to coastal diatoms by significantly lowering PSI and Cyt b_6f levels (Strzepek and Harrison 2004). Thus, one explanation which has not been considered in previous studies of *C*. sp. UWO241 is that permanent downregulation of PSI may reflect adaptive strategy to survive long-term Fe-limitation in its natural habitat.

Recently, a second psychrophilic *Chlamydomonas, C*. sp. ICE-MDV, was isolated from east lobe Lake Bonney (ELB) (Raymond and Morgan-Kiss 2017; Li et al. 2016). In contrast with *C*. sp. UWO241 which was isolated from the hypersaline deep photic zone of ELB (temperature ~ 5 °C; specific conductivity at 15 °C > 6 S m^{-1}), *C*. sp. ICE-MDV dominates the shallow photic zone where it is exposed to higher irradiance, extreme oligotrophy, and low salinity (temperature ~ 2 °C; specific conductivity at 15 °C < 0.2 S m^{-1}) (Dolhi et al. 2015; Kong et al. 2012; Spigel and Priscu 1998). The natural light levels of ELB are extreme shade enriched in blue-green wavelengths (Neale and Priscu 1995). Natural PAR levels experienced by *C*. sp. ICE-MDV (~ 50 µmol m^{-2} s^{-1}) are fivefold to tenfold higher compared with that of *C*. sp. UWO241 (< 10 µmol m^{-2} s^{-1}) (Kong et al. 2012). Cold adaptation in both ELB isolates involves expression of multiple isoforms of ice-binding proteins when grown under low temperature (Raymond and Morgan-Kiss 2013, 2017). However, it is unknown whether *C*. sp. ICE-MDV shares other phenotypic characteristics with *C*. sp. UWO241. More specifically, does *C*. sp. ICE-MDV exhibit remodeling of the photosynthetic apparatus, downregulation of PSI and high rates of PSI-associated CEF?

We hypothesize that constitutive downregulation of PSI in *C*. sp. UWO241 may reflect adaptation to permanent Fe-deficiency in ELB. Furthermore, as *C*. sp. ICE-MDV was also isolated from ELB, we further predict that this psychrophile might share some of the unique characteristics as previously described in *C*. sp. UWO241. To test these predictions, we compared PSII and PSI photochemical function in the ELB isolates (*C*. sp. UWO241 and *C*. sp. ICE-MDV) and the model alga *C. reinhardtii* grown under standard growth conditions as well as a gradient of Fe, ranging from deficient (2 µM Fe^{2+}) to excess (200 µM Fe^{2+}). We also compared the proteome of *C*. sp. UWO241 grown in standard growth medium (18 µM Fe^{2+}) versus Fe-excess (200 µM Fe^{2+}) conditions. Our results revealed that both psychrophiles altered photochemical function in response to Fe-availability; however, *C*. sp. UWO241 is distinct from both *C. reinhardtii* and *C*. sp. ICE-MDV because it maintains the unique features at the level of PSI regardless of Fe concentration. The psychrophilic *C*. spp. UWO241 and ICE-MDV represent a unique opportunity for further analyses into how long-term isolation under a suite of extreme environmental conditions can lead to different survival strategies among the extremophilic algae.

Materials and methods

Strains and growth conditions

The mesophilic *Chlamydomonas reinhardtii* (SAG11-32c) was obtained from the *Chlamydomonas* Resource Center. The psychrophilic *Chlamydomonas* sp. UWO241 (CCMP1619) was originally isolated by J Priscu in 1995 from the deep photic zone (17 m sampling depth) of ELB (Neale and Priscu 1995). The psychrophilic *Chlamydomonas* sp. ICE-MDV was isolated in 2014 from an enrichment culture of 15 m ELB water (Raymond and Morgan-Kiss 2017). Both of the ELB psychrophiles are stored in a low temperature culture laboratory at Miami University and are maintained at low temperatures (4 °C). Cultures for all experiments were grown in acid-washed 250 mL Pyrex tubes in temperature-regulated aquaria and bubbled with sterile air (Morgan-Kiss et al. 2008). The mesophilic and psychrophilic strains were grown under temperature/irradiance regimes of 20 °C/100 µmol^{-2} s^{-1} and 8 °C/100 µmol^{-2} s^{-1}, respectively. For standard conditions, cultures were grown in Bold's Basal Medium (BBM) (Bold 1949) which contained an $FeSO_4$ concentration of 18 µM Fe^{2+}. In iron treatment experiments, cultures were grown in BBM supplemented with the following $FeSO_4$ concentrations: (i) deficient = 2 µM Fe^{2+}, (ii) replete = 20 µM Fe^{2+}, and (iii) excess = 200 µM Fe^{2+}. Iron

treatments were defined based on previous studies in *C. reinhardtii* (Glaesener et al. 2013). Growth was monitored as change in optical density at 750 nm according to Morgan et al. (1998).

For phylogenetic analysis, a fragment of 18S rRNA was amplified using universal primers (Bielewicz et al. 2011) from genomic DNA isolated from mid-log cultures of *C.* sp. ICE-MDV. A purified PCR product was sequenced at the Center for Bioinformatics and Functional Genomics at Miami University. Comparative sequences of representative Chlamydomonas lineages were selected from GenBank, and closely affiliated sequences were identified using BLASTN search. Alignment of DNA sequences was performed with ClustalW in Mega7 (Kumar et al. 2016). A neighbor-joining analysis was performed, and bootstrap consensus tress (500 pseudoreplicates) were generated using the Maximum Likelihood method based on the Tamura-Nei model (Tamura et al. 2004).

Chlorophyll a and b concentrations were determined from whole cell extractions in 90% acetone according to Jeffry and Humphrey (1975).

Microscopy

A Zeiss LSM-170 confocal laser scanning microscope was used to generate images of *C.* spp. UWO241 and ICE-MDV. A 488-nm argon ion laser was used as an excitation source, and chlorophyll fluorescence was detected at 650–750 nm. Differential interference contrast images were generated using the transmission light mode.

Chlorophyll a fluorescence

Room temperature Chl *a* fluorescence was measured *in vivo* in exponentially growing cultures using a Dual-PAM 100 fluorometer (Hienz Walz GmbH, Effeltrich, Germany). Before each measurement, 10 mM $NaCO_3$ was added and the sample was exposed to far red light for 2 min to fully oxidize the photosynthetic electron transport chain. The fluorescence parameters F_V/F_M (maximum photochemical efficiency), qP (photochemical quenching or proportion of open PSII reaction centers), Y(PSII) (quantum yield of photochemistry), Y(NPQ) (nonphotochemical energy dissipation from antenna quenching) and Y(NO) (energy dissipation from nonregulated processes) were calculated during steady-state photosynthesis at the growth temperature/irradiance/iron regimes.

Low-temperature (77 K) Chl *a* emission spectra were collected on a LS50B Luminescence Spectrometer (Perkin Elmer, Buckinghamshire, England) equipped with a sample holder for liquid nitrogen (Morgan et al. 1998). Samples from mid-log phase cultures were dark adapted for 10 min at the growth temperature and flash frozen in liquid nitrogen. Frozen samples were exposed to an excitation wavelength of 436 nm. Emission spectra were collected using excitation and emission slit widths of 4 nm. Spectra are the average of three scans per replicate. Decompositional analysis of 77 K fluorescence emission spectra was performed using a nonlinear least squares algorithm using Microcal OriginPro version 8.5.1 (Microcal Origin Northampton, MA). The fitting parameters for the Gaussian components (position, area and full width half-maximum, FWHM) were free running parameters.

Measurements of PSI parameters

Photooxidation of P700 was measured as the far-red light-induced changes in absorption at 820 nm (ΔA_{820}) on the DUAL-PAM instrument (Ivanov et al. 1998; Morgan-Kiss et al. 2005). Samples of exponentially growing cultures were dark adapted for 10 min at the growth temperature. A volume of culture (5–10 mL) representing 25 µg total Chl *a* per sample was concentrated by vacuum filtration onto a Whatman GF/C 25 mm filter and attached to the fluorometer using the leaf attachment. The proportion of photooxidizable P700 ($\Delta A_{820}/A_{820}$) was determined as the change in absorbance at 820 nm after turning on the far red light (λ_{max} = 715 nm, 10 Wm^{-2}, Scott filter RG 715). Once the signal reached a steady state in the presence of far red (FR) light, single (ST) and multiple (MT) turn-over flashes (parameters) were used to determine the MT/ST ratio, representing the intersystem electron pool size. The half-time for the reduction of $P700^+$ to P700 ($t_{½}^{red}$) was calculated after the FR light was turned off to estimate relative rates of alternative electron flow around PSI (Ivanov et al. 1998; Morgan-Kiss et al. 2005). P700 photooxidation was also measured under white actinic light (AL) (200 µmol m^{-2} s^{-1}) in the presence and absence of 40 µM DCMU to estimate the contribution of electrons from PSII (Ivanov et al. 2012).

Quantum yields of energy conversion in PSI, or PSI energy partitioning, were measured on the Dual-PAM instrument according to Pfündel et al. (2008). PSI effective photochemical quantum yield was calculated as $[Y(\mathrm{I})] = \left(P'_m - P\right)/P_m$. Donor side limitation [Y(ND) = $(P-P_o)/P_m$] represents energy dissipation due to a shortage of electron donors. Acceptor side limitation $\left[Y(\mathrm{NA}) = \left(P_m - P'_m\right)/P_m\right]$ represents energy dissipation due to a shortage of electron acceptors.

Thylakoid isolation

Thylakoid membrane isolation was performed according to Morgan et al. (1998). Cell pellets from mid-log phase cultures were resuspended in Tricine-NaOH buffer (pH 7.8) containing 0.3 M sorbitol, 5 mM $MgCl_2$, 10 mM NaCl and 1 mM Pefabloc (Sigma–Aldrich). Cells were broken by

passing twice through a chilled French Pressure Cell (10,000 psi). The lysate was washed twice in Tricine buffer in the absence of sorbitol. Glycerol (10%) was added to samples before flash freezing in liquid N_2 and stored at − 80 °C.

SDS–PAGE and immunoblotting

Thylakoid samples were solubilized by boiling for 2 min in 60 mM Tris buffer (pH 7.8) containing 1 mM EDTA, 12% (w/v) sucrose and 2% SDS). Total protein was quantitated using a Bradford protein assay kit (Biorad). Thylakoid proteins were loaded on an equal protein basis (10 µg) and separated on TGX FastCast™ SDS–PAGE polyacrylamide gels (Bio-Rad). Gels were transferred to methanol-activated PVDF membranes using a TransBlot Turbo™ Transfer System (Bio-Rad). Transferred membranes were blocked overnight in 5% nonfat milk and probed with primary antibodies (Agrisera, Sweden) against the PSI reaction center protein, PsaA (Cat No. AS06-172), D1 protein, PsbA (Cat No. AS01-016), and Ferredoxin, Fdx1 (Cat No. AS06-121). Membranes were then exposed to Protein A conjugated to horseradish peroxidase, and blots were detected with ECL Select™ Western Blotting Detection Reagent (Amersham).

Proteomic analyses by liquid chromatography-tandem mass spectrometry (LC-MS/MS)

Proteomics analyses were conducted following a similar procedure in our previous work (Wang et al. 2016). Briefly, mid-log phase cultures of *C*. sp. UWO241 grown in either BBM (18 µM Fe^{2+}) or iron excess (200 µM Fe^{2+}) media were harvested by centrifugation. 100 µg of total protein from each sample was subjected to denaturing by 8 M urea and digestion using Trypsin Gold (Promega, Madison, WI) with 1:50 w/w at 37 °C for 18 h. The digested peptides were further cleaned up using a Sep-Pak C18 plus column (Waters Corporation, Milford, MA). The Multidimensional Protein Identification Technology (MudPIT)-based shotgun proteomics were performed by loading digested peptides onto a biphasic strong cation exchange/reversed phase capillary column. The two-dimensional (2D)-LC-MS/MS was conducted on a LTQ ion trap mass spectrometer (Thermo Finnegan, San Jose, CA) operated in the data-dependent acquisition mode by recording the full ass spectra of 300–1700 m/z, and fragment the 5 most abundant peaks of each scan for MS/MS analysis. The MS/MS raw data were analyzed by first converting into MS2 files, followed by database search using ProLuCID (Xu et al. 2006). The UWO 241 protein database was generated based on our transcriptomics data supplemented with 37 common contaminants and their reversed sequences as quality control system to restrain false positive discovery to 0.05. Differentially expressed proteins were analyzed using PatternLab for Proteomics (Carvalho et al. 2008). The proteomics raw data have been deposited to the ProteomeXchange Consortium via the PRIDE (Vizcaíno et al. 2015) partner repository with the dataset identifier PXD010433.

Supercomplex isolation

Sucrose density centrifugation was performed to visualize major chlorophyll–protein complexes as described by Szyska-Mroz et al. (2015) with some modifications. Mid-log phase cultures (500 ml) of *C*. sp. UWO241 grown under deficient (2 µM Fe^{2+}), replete (20 µM Fe^{2+}) or excess (200 µM Fe^{2+}) iron conditions were pelleted and washed twice in Buffer 1 (0.3 M Sucrose, 25 mM Hepes-KOH [pH 7.5], 1 mM $MgCl_2$). The resuspension was passed through a chilled French Press as described above. Broken cells were pelleted, resuspended in Buffer 2 (0.3 M Sucrose, 5 mM Hepes-KOH [pH 7.5], 10 mM EDTA) and centrifuged at 50,000xg for 30 min. Thylakoid pellets were resuspended gently in Buffer 3 (1.8 M Sucrose, 5 mM Hepes-KOH [pH 7.5], 10 mM EDTA) and transferred to a thin-walled, ultra-clear 14 ml tube (Cat No. 344,060, Beckman Coulter, USA). The thylakoid prep was overlaid with Buffer 4 (1.3 M Sucrose, 5 mM Hepes-KOH [pH 7.5], 10 mM EDTA) followed by Buffer 5 (0.5 M Sucrose, 5 mM Hepes-KOH [pH 7.5]) and centrifuged at 288,000×*g* for 1 h at 4 °C in a Sw40Ti rotor (Beckman coulter, USA). Pure thylakoids were extracted from the gradient and diluted in Buffer 6 (5 mM Hepes-KOH [pH 7.5], 10 mM EDTA) and centrifuged at 50,000×*g*. For supercomplex isolation, the membrane (0.4 mg total chlorophyll) was resuspended in solubilization buffer containing 1% n-dodecyl-alpha-maltoside (α-DDM) (Cat No. D99020, Glycon Biochemicals, Germany) and incubated on ice for 25 min. Solubilized membranes were loaded onto a linear sucrose gradient (0.1–1.3 M sucrose) containing 0.05% α-DDM. Gradients were centrifuged at 40,000 rpm for 21 h at 4 °C. Representative gradients are shown in Fig. 9S.

Results

Phylogenetic analysis and cell morphology of *C.* spp. UWO241 and ICE-MDV

Phylogenetic analyses showed that *Chlamydomonas* sp. ICE-MDV is part of the *C. pulsatilla* clade. *C*. sp. ICE-MDV is closely related to other psychrophilic Chlamydomonas, including two Antarctic marine species, *C*. sp. ICE-L and *C*. sp. ICE-W (Fig. 1S). *Chlamydomonas* sp. UWO241 is closely affiliated with the marine strain, *C. parkae*. *C*. sp. UWO241 is closely related to psychrophilic snow alga

(*Chlamydomonas* sp. 75.94) and a halotolerant strain (*Chlamydomonas* sp. HS-5) (Fig. 1S). The two ELB psychrophiles are not closely affiliated with each other genetically; however, *C*. sp. UWO241 is more closely related to *C. reinhardtii* SAG 11–32c.

Microscopic examination of the psychrophiles grown under standard growth conditions revealed that cells of both *C*. spp. UWO241 and ICE-MDV are biflagellate, ovoid and exhibit relatively high abundance of lipid bodies (Fig. 2S). The average cell size of *C*. sp. ICE-MDV (15–20 µm × 10–15 µm) was larger than that of *C*. sp. UWO241 (10–15 µm × 5–8 µm) (Table 1).

Chlamydomonas. spp. UWO241 and ICE-MDV exhibit altered photochemistry under standard growth conditions

Chlamydomonas. sp. UWO241 has been highly studied for > 20 years and is a model for cold-adaptation of photosynthesis (see reviews by Cvetkovska et al. 2017; Dolhi et al. 2013; Morgan-Kiss et al. 2006). While *C*. sp. UWO241 resides in the deep photic zone (Neale and Priscu 1990), *C*. sp. ICE-MDV dominates the oligotrophic shallow layers of ELB (Kong et al. 2012). Both ELB isolates are true psychrophiles and therefore exhibited comparable growth responses to low temperature (Table 1). Under standard growth conditions (BBM; temperature/light regime of 8 °C/100 µmol m^{-2} s^{-1} and 20 °C/100 µmol m^{-2} s^{-1} for the ELB psychrophiles and mesophilic *C. reinhardtii* cultures, respectively), growth rates of both psychrophile strains *C*. spp. UWO241 and ICE-MDV were ~ 50% lower relative to that of the mesophile *C. reinhardtii* (Table 1). Mid-log phase cultures for all strains exhibited high PSII photochemical efficiency (F_V/F_M) and PSII oxidation state (qP) values. Despite comparable PSII photochemistry, both psychrophile strains exhibited significantly higher cellular Chl levels compared to the mesophile *C. reinhardtii* (Table 1).

Low-temperature (77 K) Chl *a* fluorescence emission spectra were monitored as an estimate of energy distribution between PSII and PSI (Fig. 1a). *C. reinhardtii* cultures grown under control conditions exhibited a typical 77 K fluorescence emission spectrum with Chl *a* fluorescence emission peaks at 685 nm (F_{685}) and 715 nm (F_{715}), representing light harvesting complex (LHCII) and PSI fluorescence, respectively (Fig. 1a) (Krause and Weis 1991). In contrast with *C. reinhardtii* and in agreement with previous reports (Morgan et al. 1998; Szyszka et al. 2007), *C*. sp. UWO241 lacked a defined F_{715} peak (Fig. 1a). Conversely, *C*. sp. ICE-MDV exhibited a 77 K emission spectrum which resembled that of *C. reinhardtii* with prominent peaks at F_{685} and F_{715} (Fig. 1a).

Functional measurements of PSI were taken by monitoring far red light (FR)-inducible P700 photooxidation (Fig. 1b–d). *C. reinhardtii* exhibited an expected P700 induction curve (Fig. 1b) which matched those from published reports (Morgan-Kiss et al. 2005). An increase in A_{820} was detected following FR illumination, indicating oxidation of P700 to $P700^+$. Flashing of the ST and MT actinic light (AL) source induced partial and full transitory reduction in $P700^+$ to P700, respectively. $P700^+$ was re-reduced back to P700 once the FR light was turned off (Fig. 1b). Cultures of *C*. sp. UWO241 grown under standard conditions exhibited relatively low FR-induced photooxidation of P700 to $P700^+$, and transitory reduction of $P700^+$ by ST and MT was undetectable (Fig. 1c). In contrast, *C*. sp. ICE-MDV exhibited a P700 induction curve which was more comparable with that of *C. reinhardtii* than s *C*. sp. UWO241 (Fig. 1d).

While FR light exclusively excites PSI, P700 measurements in the presence of white AL reflect excitation of PSI and PSII. To investigate the contribution of linear electron transport from PSII to P700, A_{820} was monitored under AL (200 µmol m^{-2} s^{-1}) and in the presence or absence of the PSII inhibitor, DCMU (Table 2). In the absence of DCMU, electrons from PSII resulted in a $\Delta A_{820}/A_{820}$ which was 1.45-fold higher in *C*. sp. UWO241 compared with *C. reinhardtii* and *C*. sp. ICE-MDV. In contrast, when electrons from PSII were blocked by DCMU, both *C. reinhardtii* and *C*. sp. ICE-MDV exhibited an increase in $\Delta A_{820}/A_{820}$ (2.0- and 1.6-fold, respectively), while DCMU-treated cells of *C*. sp. UWO241 exhibited no change in $\Delta A_{820}/A_{820}$ (Table 2). These results indicate that the contribution of electrons from linear electron transport is relatively low in *C*. sp. UWO241, relative to *C. reinhardtii* and *C*. sp. ICE-MDV. Together with the results from the 77 K fluorescence spectra, the P700

Table 1 Growth rates and photosynthetic parameters of *C. reinhardtii*, C. sp. UWO241, and *C*. sp. ICE-MDV grown under control conditions

Species	Growth rate (day^{-1})	F_V/F_M	Chl a/b ratio (mol/mol)	Chl/cell (pmol $cell^{-1}$)	Cell size (µm)
C. reinhardtii	0.50 ± 0.14	0.78 ± 0.01	2.58 ± 0.22	0.23 ± 0.06	9.0 ± 1.0
C. sp. UWO241	0.27 ± 0.05	0.70 ± 0.00	2.04 ± 0.24	1.96 ± 0.59	12 ± 2.5
C. sp. ICE-MDV	0.26 ± 0.04	0.75 ± 0.00	2.24 ± 0.14	3.41 ± 0.63	17 ± 2.3

All strains were grown in Bold's medium and moderate light levels (100 µmol m^{-2} s^{-1}). *C. reinhardtii* was grown at 20 °C, and the psychrophiles were grown at 8 °C. F_V/F_M, maximum photochemical efficiency

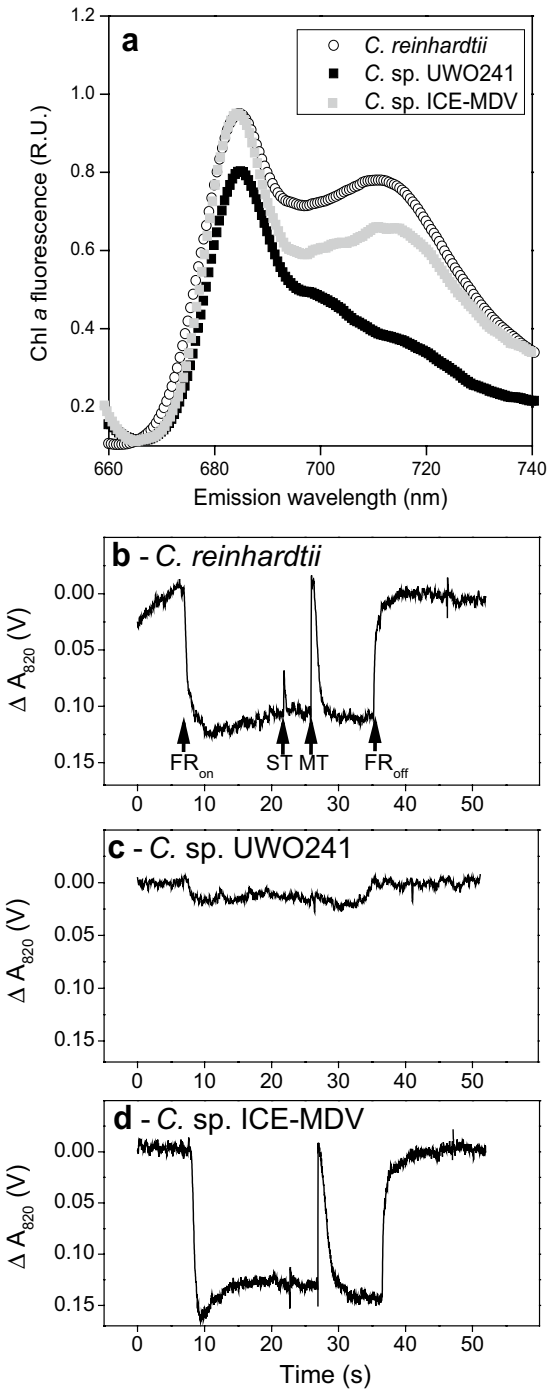

Fig. 1 Comparison of photosystem I functional characteristics of mesophilic and psychrophilic algal cultures grown under standard conditions (20 °C/100 μmol^{-2} s^{-1} and 8 °C/100 μmol^{-2} s^{-1}, respectively). Representative traces of low temperature (77 K) fluorescence emission spectra (**a**) and PSI oxidation/reduction kinetics (**b**–**d**) of *C. reinhardtii, C.* sp. UWO241, and *C.* sp. ICE-MDV grown under standard conditions in Bold's Basal Medium (BBM). **b**–**d** P_{700}^{+} oxidation/reduction kinetics of *C. reinhardtii* (**b**), *C.* sp. UWO241 (**c**), and *C.* sp. ICE-MDV (**d**). The iron concentration in BBM was 18 μM Fe^{2+}. All values represent normalized data

oxidation–reduction results indicate that despite exhibiting similar growth physiology under standard conditions, functional organization of PSI appears to be significantly different between the two ELB species.

Natural Fe levels in Lake Bonney

Iron concentrations in ELB have not been measured routinely. Past reports have noted that total iron levels in the upper photic zone are near or below the levels of detection of the methods used (~ 180 nM (Weand et al. 1976; Angino et al. 1964; Armitage and House 1962; Ward et al. 2003). To our knowledge, the only published profiles of total iron in ELB were determined using atomic absorption spectrometry (Weand et al. 1976), Fig. 3S). Samples for these measurements were collected during the 1974–1975 austral summer (November to January) in the eastern portion of ELB when the lake levels were about 8 meters lower than they are today. Using data on lake levels collected routinely as part of the McMurdo LTER program, we were able to estimate the total iron levels in1989 and 2014 when *C.* spp. UWO241 and ICE-MDV were isolated, respectively. Assuming that most of the iron in the photic zone is derived from upward diffusion across the chemocline and that photic zone losses are constant over time, we estimate total iron levels of 9.7 and 1.1 μM for the water layer where these respective organisms were originally collected. The availability of this iron to phytoplankton not only depends on total concentration but also its chemical speciation, cellular C:Fe ratios, and the physiochemical properties of the system that alter speciation (Molot and Dillon 2003; Shaked et al. 2004). Unfortunately, no such information exists for ELB. Although most studies of Fe-deficiency in phytoplankton have focused on marine systems (e.g., Frost and Franzen 1992; Martin 1992; Behrenfeld et al. 1996), Morton and Lee (Morton and Lee 1974) and Pollingher et al. (1995) have shown that total iron concentrations between 1.8 and 18 μM can alter community composition of the phytoplankton in lakes.

Effect of Fe on growth physiology and photosynthesis

Given the striking differences in apparent PSI functional organization between the ELB psychrophiles *C.* spp. UWO241 versus ICE-MDV and that PSI downregulation is a major target when cells are exposed to limiting iron (Merchant et al. 2006), we tested whether differential Fe requirements could account for these marked differences in the photochemical apparatus. Cultures were grown under the standard temperature/irradiance regimes described above, with the exception that BBM-Fe was supplemented with variable iron to represent: (i) Fe-deficient (2 μM Fe^{2+}), (ii) Fe-replete (20 μM Fe^{2+}), or (iii) Fe-excess

Table 2 Effects of DCMU on P700 oxidation in white actinic light excitation (200 µmol m^{-2} s^{-1})

Strain	$\Delta A_{820}/A_{820}$		Absorbance change ratio in +DCMU versus −DCMU
	−DCMU	+ DCMU	
C. reinhardtii	0.064 ± 0.020	0.131 ± 0.042	2.04
C. sp. UWO241	0.093 ± 0.020	0.092 ± 0.037	0.98
C. sp. ICE-MDV	0.064 ± 0.014	0.105 ± 0.015	1.64

Cultures were grown under control growth conditions

(200 µM Fe^{2+}). Growth rates of *C.* spp. UWO241 and ICE-MDV were comparable across all Fe-treatments, with the exception that Fe-deficient cultures of *C.* sp. UWO241 exhibited a 1.5-fold lower growth rate compared with Fe-replete or Fe-excess conditions (Fig. 4S). Absorption spectra of isolated thylakoid membranes for all three strains grown under variable Fe is shown in Fig. 5S. In general, all strains exhibited an increase in absorbance in the blue region of the spectra in response to increasing Fe.

F_V/F_M remained high in *C. reinhardtii* regardless of Fe treatment (Fig. 2a). Both psychrophiles exhibited a moderate reduction in F_V/F_M when grown under Fe-deficient conditions (Fig. 2a). qP also remained high across all strains (Fig. 2b). However, all three strains exhibited higher sensitivity to Fe deficiency at the level of the effective quantum yield of PSII [*Y*(PSII)] (Figs. 2c, 3a, c, e). Last, while both psychrophiles exhibited higher NPQ values across all Fe treatments relative to *C. reinhardtii* (Fig. 2d), Fe-deficient cultures of *C.* sp. UWO241 exhibited significantly higher *Y*(NPQ) (Fig. 3c), while cultures of both *C. reinhardtii* and *C.* sp. ICE-MDV exhibited

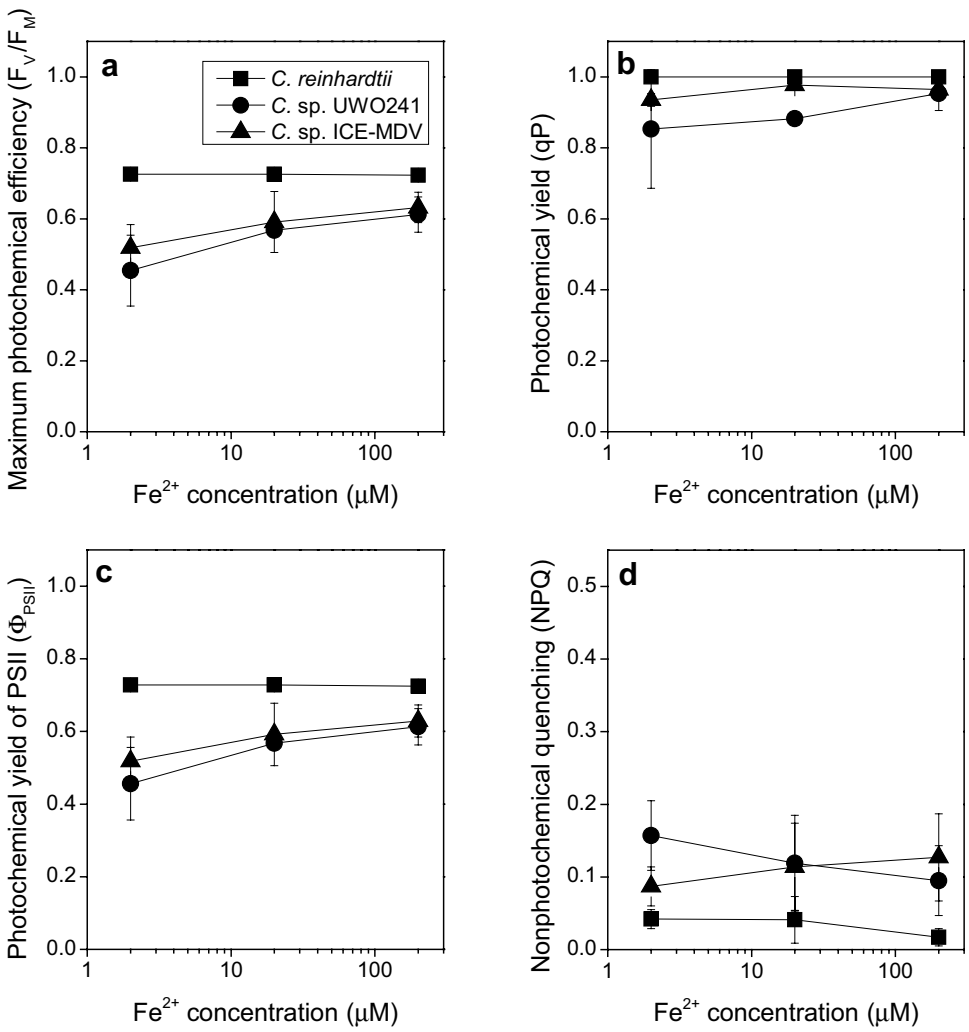

Fig. 2 Effects of iron concentration on maximum photochemical efficiency of PSII (F_V/F_M, **a**), photochemical quenching (qP, **b**), photochemical yield of PSII (ϕ_{PSII}, **c**), and nonphotochemical quenching (NPQ, **d**) in cells of *C. reinhardtii, C.* sp. UWO241, and *C.* sp. ICE-MDV. Cultures were grown under varying concentrations of Fe^{2+}. Values are means ± SD (n = 3)

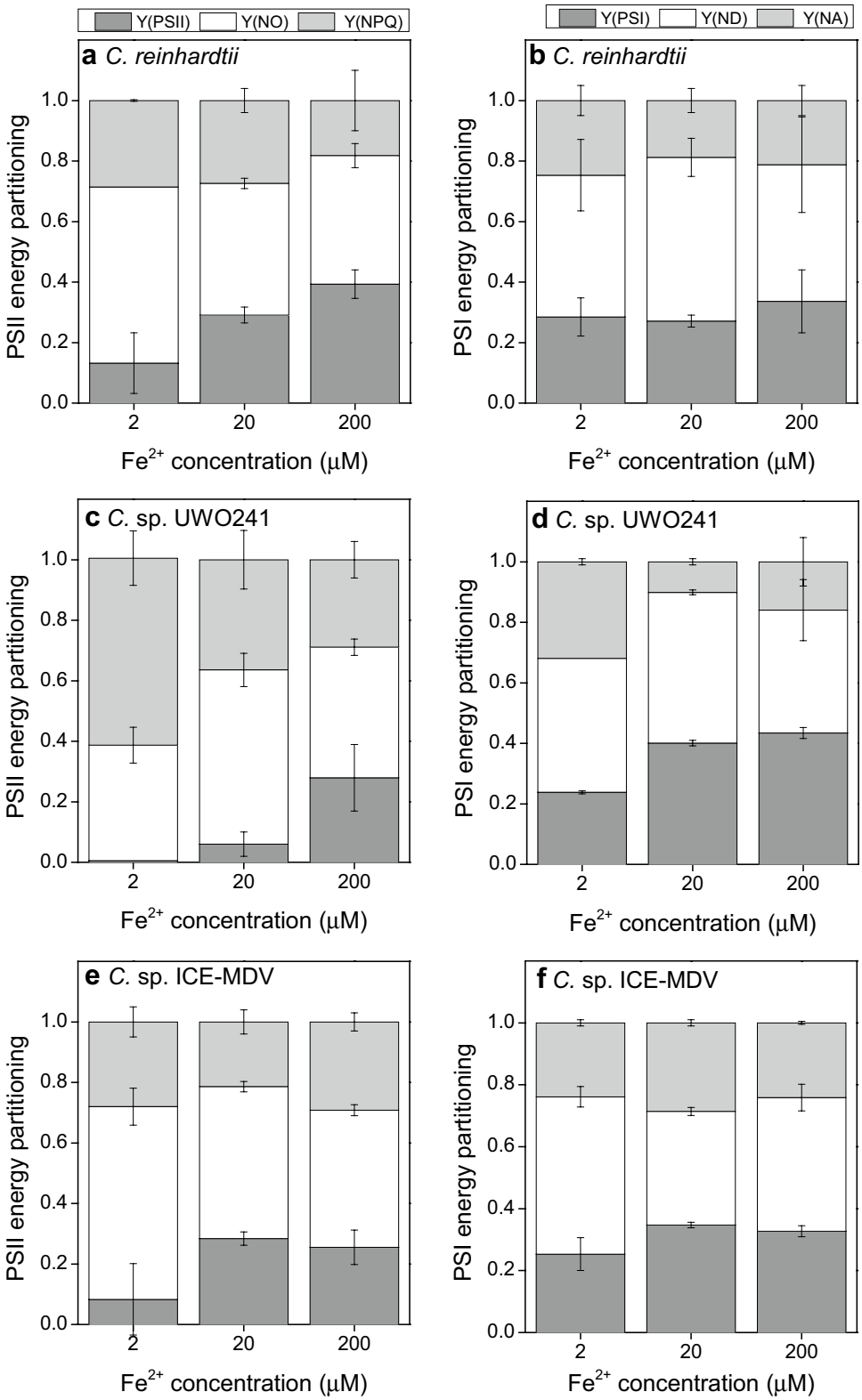

Fig. 3 Effect of iron concentration on energy partitioning in PSII and PSI in *C. reinhardtii* (**a, b**), *C*. sp. UWO241 (**c, d**), and *C*. sp. ICE-MDV (**e, f**). Y(PSII), photochemical yield of PSII; Y(NO), nonregulated energy dissipation; Y(NPQ), nonphotochemical quenching; Y(PSI), photochemical yield of PSI; Y(ND), donor-side limitation of PSI; Y(NA), acceptor-side limitation of PSI. Values are means ± SD ($n = 3$)

higher nonregulated energy dissipation [*Y*(NO), Fig. 3a, e].

Effect of Fe on PSI function

To investigate whether there were differential impacts of Fe availability on PSI structure/function, 77 K fluorescence

emission spectra and P700 photooxidation kinetics were performed in all three strains grown under all Fe-treatments. At the level of 77 K fluorescence emission, Fe-deficiency induced a reduction in F_{715} across all three strains (Fig. 4), suggesting functional and/or structural downregulation of PSI. However, when grown under Fe-excess, cultures of *C. reinhardtii* and *C.* sp. ICE-MDV exhibited a recovery of PSI (F_{715}) fluorescence (Figs. 4a, c, 5), while *C.* sp. UWO241 appeared to be minimally impacted by Fe concentration (Figs. 4b, 5). Moreover, *C.* sp. UWO241 exhibited a prominent peak at 695 nm (F_{695}) under both Fe-replete and -excess conditions (Fig. 4b).

Decompositional analysis was performed on the 77 K fluorescence emission spectra of all strains grown under Fe-deficient versus Fe-replete conditions (Table 3; Fig. 6S). A best fit for all samples ($R^2 > 0.999$) was attained with four major spectral components corresponding to 683–685 nm (LHCII), 696–699 nm (PSII core complex), 708–711 nm (PSI) and 735–738 nm (near-infrared vibrational transitions) (Morgan-Kiss et al. 2002a). While all strains exhibited peak positions within the expected range, the relative area of the subbands was strain specific and dependent upon Fe availability. Regardless of the Fe treatment, *C.* sp. UWO241 showed significantly lower subband areas corresponding to the PSI core complex compared to *C. reinhardtii* and *C.* sp. ICE-MDV (Table 3). However, in response to increased Fe availability, *C.* sp. UWO241 cells grown under Fe-excess conditions exhibited a 1.7-fold increase in PSI-associated band area which was comparable to *C. reinhardtii* (Table 3). In contrast with *C.* sp. UWO241, *C.* sp. ICE-MDV exhibited no change in the relative band area of PSI in Fe-excess versus Fe-deficient conditions. Instead, Fe-excess cells of *C.* sp. ICE-MDV exhibited a 1.45-fold decline in the LHCII-associated band area at 684 nm (Table 3). Thus, in response to an increase in iron availability, all strains responded

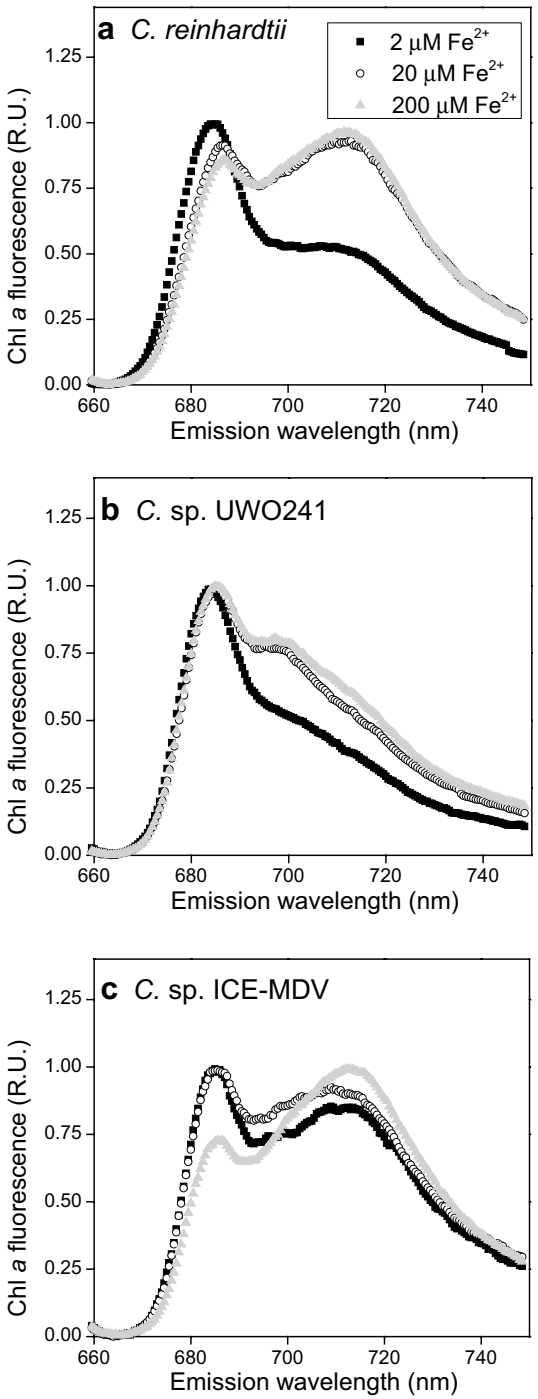

Fig. 4 Low-temperature (77 K) fluorescence emission spectra of *C. reinhardtii* (**a**), *C.* sp. UWO241 (**b**) and *C.* sp. ICE-MDV (**c**) grown under varying concentrations of iron. All spectra represent the average of nine measurements

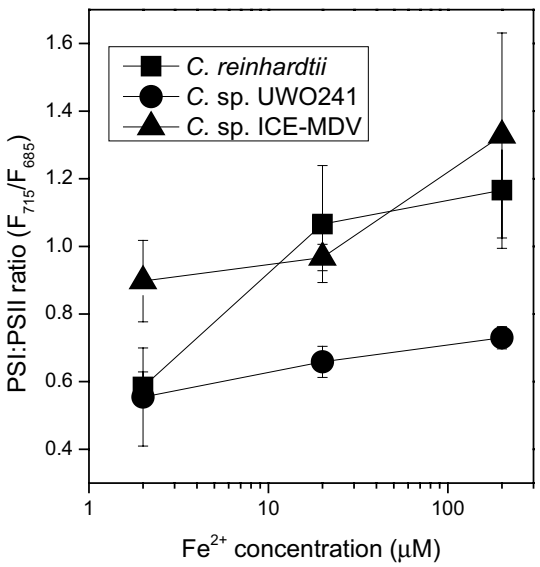

Fig. 5 PSI/PSII ratios of *C. reinhardtii, C.* sp. UWO241 and *C.* sp. ICE-MDV grown under varying concentrations of iron. Values represent the ratio of F_{715}/F_{685} generated from 77 K fluorescence emission peak heights in Fig. 4. Values are means ± SD ($n = 3$)

Table 3 Gaussian fitting parameters for subband decomposition of 77 K Chl a fluorescence emission spectra from cultures grown under Fe-deficient (2 µM Fe^{2+}) versus Fe-excess (200 µM Fe^{2+}) conditions

Subband	*C. reinhardtii*		*C.* sp. UWO241		*C.* sp. ICE-MDV	
	Fe-deficient	Fe-excess	Fe-deficient	Fe-excess	Fe-deficient	Fe-excess
1 λ_{Max}	683.7	685.3	682.8	683.6	684.0	684.0
FWHM	14.99	15.17	12.64	13.13	12.40	12.23
Area %	13.12	9.52	8.80	10.08	8.20	5.64
2 λ_{Max}	698.1	698.5	694.1	696.3	695.9	696.0
FWHM	10.54	10.30	19.33	14.89	10.45	14.26
Area %	1.10	1.40	5.72	5.01	1.48	2.84
3 λ_{Max}	708.8	710.4	709.0	707.9	709.6	711.4
FWHM	30.90	30.01	27.55	28.71	32.27	28.51
Area %	14.20	22.95	7.44	13.19	18.99	18.67
4 λ_{Max}	736.9	737.5	735.6	734.7	738.5	734.9
FWHM	39.97	42.93	44.38	48.11	45.84	44.78
Area %	6.17	10.91	4.77	9.67	9.75	12.06
R^2	0.9998	0.9998	0.9998	0.9998	0.9994	0.9998

Percentage represents the ratio of subband 3 to subband 1 in Fe-excess versus Fe-deficient conditions. Analysis was performed on the means of 9 replicates per sample

with a redistribution in energy partitioning in favor of PSI, although the overall effect on PSI/PSII fluorescence emission was most pronounced in *C. reinhardtii* (222% increase in PSI/PSII band area for Fe-excess vs. Fe-deficient cells) compared with the psychrophiles (155% and 143% for *C.* spp. UWO241 and ICE-MDV, respectively).

P700 photooxidation dynamics in response to Fe-availability were monitored as FR light-inducible ΔA_{820}. All strains exhibited low $\Delta A_{820}/A_{820}$ when grown in Fe-deficient growth media, with this effect being most pronounced in *C.* sp. UWO241 (Figs. 6a, 7S). Following FR illumination, rates of P700 + re-reduction in the dark reflect the contribution of alternative electron transport pathways, primarily PSI-associated CEF (Ravenel et al. 1994; Ivanov et al. 2012). The re-reduction time of PSI ($t_{1/2}^{red}$) was consistently slower in the mesophilic *C. reinhardtii* relative to both psychrophile strains across all conditions (1.2- to 3.8-fold higher $t_{1/2}^{red}$ in the mesophile *C. reinhardtii* vs. *C.* spp. UWO241 and ICE-MDV, respectively; Fig. 6b), suggesting that both psychrophile strains possess constitutively higher rates of CEF relative to the mesophile, regardless of the growth condition. In particular, Fe-deficiency was associated with significantly slower $t_{1/2}^{red}$ in *C. reinhardtii*, while Fe-availability had minimal impacts on $t_{1/2}^{red}$ in both psychrophile strains (Fig. 6b). The ratio of MT/ST area (e^-/P700) is an estimate of the functional electron pool size of intersystem electron transporters (Asada et al. 1992). Under all conditions, the MT and ST were undetectable in *C.* sp. UWO241 (Fig. 6c and 7S). These data agree with the P700 AL measurements under standard growth conditions, suggesting that electrons originating from intersystem electron transport are constitutively low in *C.* sp. UWO241 (Table 2). In contrast, both *C. reinhardtii* and *C.* sp. ICE-MDV exhibited relatively comparable MT/ST areas. Last, *C. reinhardtii* and *C.* sp. ICE-MDV exhibited lower MT/ST areas with reduced Fe-availability (Fig. 6c), suggesting an impairment in donor side sources of electrons in both species under Fe-deficient conditions.

In general, PSI energy partitioning was less effected by Fe availability relative to PSII (Fig. 3). However, cultures of all strains grown under Fe-deficiency exhibited a lower quantum yield of PSI [*Y*(I)] due to higher energy dissipation from both donor-side limitation [*Y*(ND)] and acceptor-side limitation [*Y*(NA)] (Fig. 3b, d, f).

Immunoblotting for major photosynthetic proteins

Given the differential functional changes in PSI between the *C.* sp. UWO241 versus *C. reinhardtii* and *C.* sp. ICE-MDV, we investigated whether PSI was also structurally downregulated in *C.* sp. UWO241. Abundance of the PSII and PSI core proteins, PsbA and PsaA, as well as the PSI electron acceptor, ferredoxin (Fd), were monitored by immunoblotting (Fig. 7). All strains exhibited reduced levels of PsbA, PsaA and Fd in response to growth under Fe-deficient conditions (Fig. 7). However, under Fe-replete conditions (i.e., 20 µM Fe), both *C. reinhardtii* and *C.* sp. ICE-MDV exhibited a significant increase in PsbA, PsaA and Fd, while levels of all three polypeptides remained low in *C.* sp. UWO241. Thus, *C.* sp. UWO241 required levels of iron > 20 µM to upregulate expression of core PSI and PSII polypeptides, while 20 µM Fe was sufficient to support maximal levels of these major photosynthetic proteins in *C. reinhardtii* and *C.* sp. ICE-MDV.

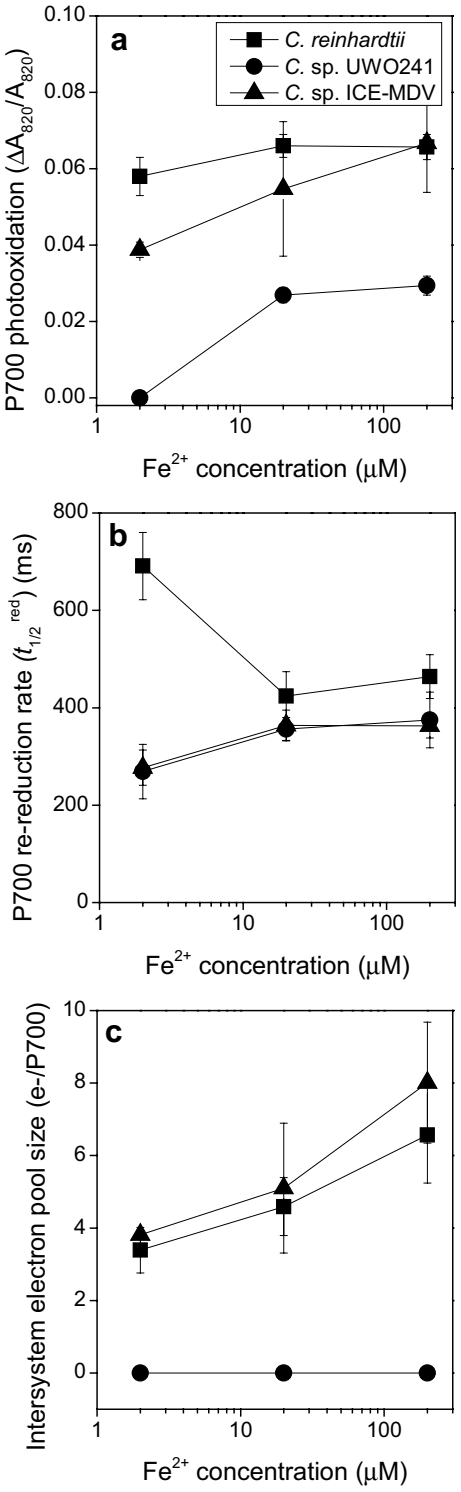

Fig. 6 Effect of iron availability on steady-state P_{700}^+ parameters in *C. reinhardtii, C.* sp. UWO241, and *C.* sp. ICE-MDV. **a** $\Delta A_{820}/A_{820}$, relative change in absorbance at 820 nm after the far red light was turned on. **b** $t_{½}^{red}$, half-time for re-reduction of P_{700}^+ after the far red light was turned off. **c** e^-/P700, relative intersystem electron pool size per P700 reaction center and was calculated as the ratio of multiple to single turn over flash. Values are means ± SD ($n = 3$)

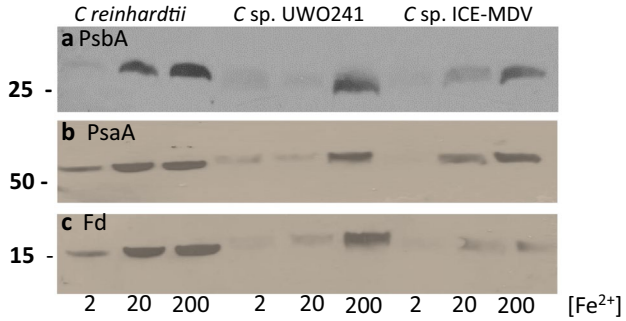

Fig. 7 Representative immunoblots of SDS–PAGE probed with antibodies against PsbA (**a**), PsaA (**b**), and Ferredoxin (Fd, **c**) in isolated thylakoids from *C. reinhardtii, C.* sp. UWO241, and *C.* sp. ICE-MDV across an iron gradient. Numbers on the left represent molecular (kD) mass of marker

Supercomplex formation in UWO241

A recent paper reported that high rates of CEF in *C.* sp. UWO241 were associated with formation of a PSI-supercomplex (Szyszka-Mroz et al. 2015). We performed sucrose density gradient ultracentrifugation on purified thylakoids from *C.* sp. UWO241 grown under variable iron (Fig. 8S). Under Fe-deficient conditions, three distinct bands were resolved, representing oligomeric LHCII (band 1), PSII core (band 2) and PSI core (band 3). A fourth, poorly resolved band was detected at the bottom of the sucrose gradient which may represent a PSI supercomplex. In contrast, thylakoids isolated from cultures grown under higher Fe lacked this heavier band (Fig. 8S).

Proteomic analyses of *C.* sp. UWO241 in standard versus Fe-excess

To further investigate the impact of iron availability on *C.* sp. UWO241, we performed a preliminary proteomic analysis of *C.* sp. UWO241 grown under Fe-excess (200 μM Fe) versus standard (BBM growth medium, 18 μM Fe) conditions. Proteins associated with the processes of photosynthesis and protein biosynthesis were most effected by Fe availability (Fig. 8). We discovered that the abundance of several key photosynthetic proteins was significantly altered under the standard versus excess Fe conditions (Fig. 9). Proteins associated with PSI core complex, LHCII and PSII core complexes, Cytochrome b_6f, as well as several subunits from the chloroplastic ATP synthase were upregulated in Fe-excess relative to standard conditions (Fig. 9). Thus, the proteomic analyses supported the results from the immunoblots that PSII and PSI core complexes are both down-regulated in *C.* sp. UWO241 under Fe-replete conditions (Fig. 7). In contrast, two proteins involved in the PSII repair cycle (HHL1 and UPF0603) were present at higher levels

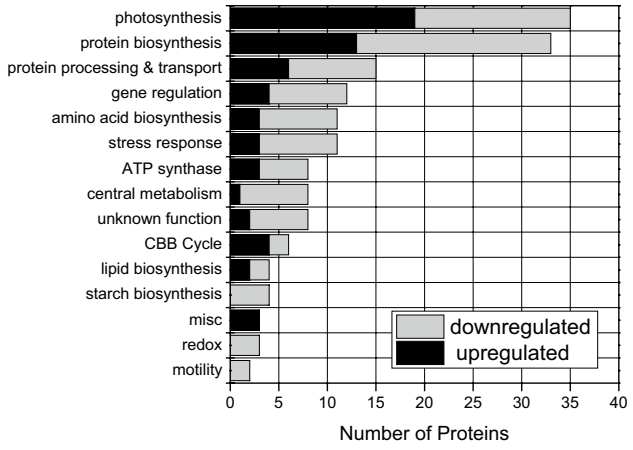

Fig. 8 Functional categories of proteins upregulated (black) or downregulated (gray) under excess Fe (200 μM Fe^{2+}) relative to standard Fe (18 μM Fe^{2+}) conditions in *C.* sp. UWO241 ($n=3$ and 2, for standard and excess Fe conditions, respectively)

in cells grown in standard growth medium compared with those grown in Fe-excess medium (Fig. 9). Five additional photosynthetic proteins were highly abundant in BBM- versus Fe-excess-grown cultures: (i) a bestrophin (BEST)-like anion channel, (ii) subunit IV of the Cyt b_6f complex (PetD), (iii) one ATP synthase subunit (AtpE) and (iv) two proteins associated with CEF, a subunit of NAD(P)H-quinone oxidoreductase (NdhS) and PGR5-like protein (PGR1) (Fig. 9). In addition, relative to Fe-excess conditions, under standard conditions *C.* sp. UWO241 exhibited high levels of three proteins involved in Ca+ signaling (Table 1S). These were a chloroplastic calcium sensing receptor (CAS) and two calcium-dependent protein kinases (CPK12 and KCC2D) (Table 1S). Last, several key enzymes from carbon metabolism pathways were upregulated under standard conditions relative to Fe-excess. These proteins included one enzyme from the CBB cycle (RbcL), four enzymes involved in starch synthesis (GlgB1, PsL5, and two isoforms of GlgS1), and three from the chorismate biosynthesis pathway (AroC, AroF, AroG) (Table 2S).

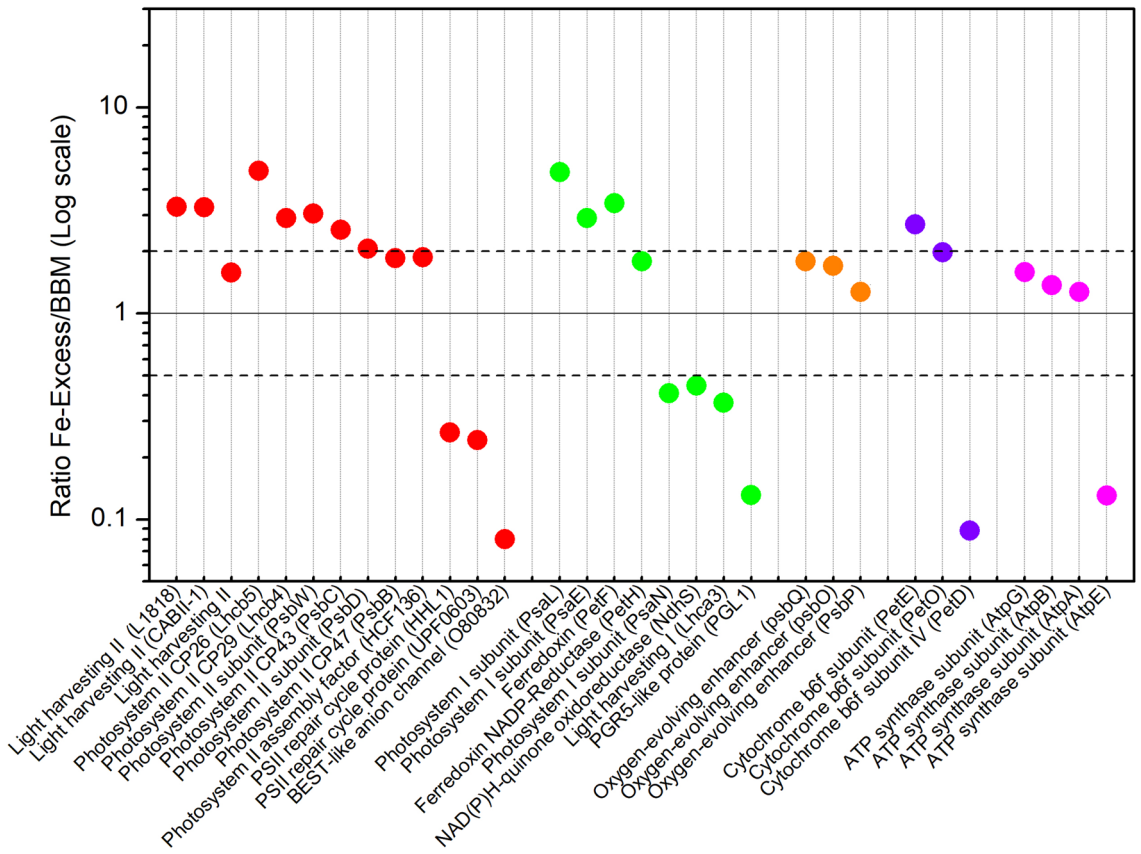

Fig. 9 Comparative quantitation of photosynthetic proteins from *C.* sp. UWO241 cultures grown under standard (18 μM Fe^{2+}) versus iron excess (200 μM Fe^{2+}) conditions. The y-axis represents the mean ratio of the respective photosynthetic proteins in standard/Fe-excess conditions. The solid line separates proteins upregulated (left) versus downregulated (right) in response to excess iron. The dashed lines visualize twofold differences ($n=3$ and 2, for standard and excess Fe conditions, respectively)

Several studies have reported that the model alga *C. reinhardtii* reorganizes the LHCI–PSI complex in response to iron availability, including changes in abundance of several of the LHCI proteins (Naumann et al. 2005, 2007). In contrast with these previous findings, we observed minimal changes in LHCI protein abundance in response to Fe-availability in the C. sp. UWO241 proteome (Fig. 9). *C. reinhardtii* possesses a large LHCI antenna complex composed of 9 Lhca Chl binding proteins (Lhca1—Lhca9) (Stauber et al. 2009). However, when we queried proteomic samples of *C.* sp. UWO241 grown under either standard or Fe-excess conditions, we were only able to identify a total of two LHCI proteins, Lhca3 and Lhca5 (Table 3S). The absence of the other LHCI proteins was not due to an inability to identify them as a search of the *C.* sp. UWO241 transcriptome identified 9 Lhca homologues (data not shown).

Discussion

Photosynthetic organisms living in permanently cold environments are often exposed to multiple environmental stressors, including chronically low iron. While the underlying mechanisms of psychrophily have been described in several model algal species (Cvetkovska et al. 2017, 2018; Morgan-Kiss et al. 2006; Zhang et al. 2018; Yi-Bin et al. 2017; La Rocca et al. 2015; Mock et al. 2017; Lukeš et al. 2014), the combined impact of long-term Fe-deficiency and low temperatures on the growth physiology of photopsychrophiles is less well understood. Our study shows that the psychrophilic *C.* spp. UWO241 and ICE-MDV respond differentially to Fe-availability. We hypothesized that the underlying mechanism for this difference in *C.* sp. UWO241 is associated with the unique function and organization of PSI, a major protein complex target during Fe-deficiency, as an adaptive strategy to survive chronic Fe-stress combined with additional environmental stressors.

One of the striking characteristics of the photosynthetic apparatus of *C.* sp. UWO241 is a downregulated PSI combined with a limited ability to significantly modulate energy distribution between PSII and PSI under various short- and long-term stress treatments (Morgan et al. 1998; Morgan-Kiss et al. 2002a, b, 2005; Szyszka et al. 2007). The inability to respond to environmental perturbation appears to be compensated in *C.* sp. UWO241 by constitutively high rates of PSI-driven CEF (Morgan-Kiss et al. 2002b) as well as a high capacity for nonregulated energy dissipation (Szyszka et al. 2007). Could these unusual phenotypic characteristics reflect adaptations shared among the algal populations which have evolved under the extreme and stable physicochemistry of ELB? Recently we reported that similar to *C.* sp. UWO241, *C.* sp. ICE-MDV requires growth temperatures < 15 °C for growth and possesses many functional isoforms of ice-binding proteins which protect these organisms from ice formation (Raymond and Morgan-Kiss 2013, 2017). Our results here demonstrate that when grown under standard conditions, both psychrophiles exhibited lower Chl *a*/*b* ratios and significantly higher Chl/cell, relative to *C. reinhardtii* (Table 1). These results are consistent with previous observations that *C.* sp. UWO241 possesses a photosynthetic apparatus which is adapted for efficient light capture under extreme shade enriched in blue-green wavelengths (Morgan et al. 1998; Neale and Priscu 1990, 1995). However, under standard growth conditions, cultures of *C.* sp. ICE-MDV exhibited a typical 77 K fluorescence emission spectrum in conjunction with significantly higher $\Delta A_{820}/A_{820}$, relative to *C.* sp. UWO241 grown under identical conditions. Moreover, $\Delta A_{820}/A_{820}$ under AL was comparably sensitive to DCMU in both the control alga *C. reinhardtii* and *C.* sp. ICE-MDV (Table 2), indicating that electrons originating from PSII contribute significantly to reduction in P700 in *C. reinhardtii* and *C.* sp. ICE-MDV. In contrast, AL-induced ΔA_{820} in cultures of *C.* sp. UWO241 was largely insensitive to DCMU, indicating that PSII and PSI are largely uncoupled in this ELB isolate. This conclusion was also supported by a lack of a measurable P700 MT/ST ratio in *C.* sp. UWO241 (Fig. 6c). These results indicate that *C.* sp. UWO241 exhibits unique features in PSI function and sources of intersystem electrons, even compared with other phytoplankton isolated from ELB.

Differences between the two psychrophile strains may be due to variations in the environment from which they were isolated. While both *C.* spp. UWO241 and ICE-MDV were isolated from ELB and should exhibit shared adaptive strategies to survive permanent low temperatures, studies on the natural populations indicate that these two species occupy different layers of the stratified photic zone. *C.* sp. UWO241 resides in the deep photic zone (17 m), where it is adapted to extreme shade and higher levels of nutrients and dissolved ions, including salinity levels higher than fivefold seawater (Neale and Priscu 1995). In contrast, populations of *C.* sp. ICE-MDV dominate the shallow photic zone (5 m) of ELB (Bielewicz et al. 2011) and reside under significantly lower salt, higher light and oligotrophic conditions compared with *C.* sp. UWO241. Past studies on *C.* sp. UWO241 suggest that adaptation to permanent low temperatures and hypersalinity are major driving factors for its unusual photobiology (Szyszka et al. 2007; Szyszka-Mroz et al. 2015). This current study extends this work by showing that two algal isolates from the same Antarctic lake exploit different adaptive strategies for surviving under permanent environmental stress.

Iron is a major environmental factor impacting the function of the photosynthetic apparatus. Since the pigment–binding protein complex PSI is a key target during growth under Fe-limiting conditions, we predicted that the unusual PSI phenotype exhibited in *C.* sp. UWO241

could be partially explained by differential effects of iron between the two ELB strains. The mesophile alga *C. reinhardtii* exhibited functional and structural downregulation of PSI at the level of 77 K fluorescence (F_{715}), photooxizable P700 levels ($\Delta A_{820}/A_{820}$) and PsaA protein. In agreement with previous reports, growth under replete levels of Fe restored PSI activity and abundance to maximal levels in the mesophile. Increased Fe-availability in cultures of *C*. sp. UWO241 resulted in a moderate recovery of PSI activity, at the level of F_{715} and $\Delta A_{820}/A_{820}$; however, the response of *C*. sp. UWO241 to iron was highly attenuated, relative to both *C. reinhardtii* and *C*. sp. ICE-MDV. These results suggested that iron requirements partially explain earlier reports that *C*. sp. UWO241 appears to exhibit a constitutively downregulated PSI (Morgan et al. 1998; Morgan-Kiss et al. 2002b; Szyszka et al. 2007).

Even under Fe-excess growth conditions, PSI 77 K fluorescence remained relatively low in *C*. sp. UWO241, despite significant increase the abundance of PsaA (Figs. 4, 7). In *C. reinhardtii*, LHCI is remodeled under Fe-stress to downregulate PSI and avoid PSI damage caused by acceptor-side limitation (Naumann et al. 2005, 2007). Thus, high PSI fluorescence in Fe-excess cultures of *C. reinhardtii* and *C*. sp. ICE-MDV is likely due to upregulation of both PSI and LHCI. Proteomic analyses of *C*. sp. UWO241 indicated that while several proteins associated with the PSI and PSII core reaction centers as well as LHCII were upregulated under Fe-excess conditions, LHCI protein abundance was not affected by iron concentration (Fig. 9). Moreover, only two LHCI proteins (Lhca3 and Lhca5, Table 2S) were detectable in the *C*. sp. UWO241 proteome (Table 3S). In *C. reinhardtii*, both Lhca3 and Lhca5 are associated with short wavelength 77 K fluorescence emission, while Lhca 2 and Lhca9 are responsible for long-wavelength fluorescence emission (Drop et al. 2011). Thus, *C*. sp. UWO241 exhibits a permanently downregulated LHCI and lacks Lhca proteins associated with long wavelength emission, accounting for the constitutively low PSI fluorescence. These results agreed with Morgan et al. (1998) who reported that *C*. sp. UWO241 (formerly called *C. subcaudata*) exhibited reduced or undetectable levels of all Lhca polypeptides. Furthermore, these authors proposed that permanent downregulation of the PSI-LHCI complex in conjunction with a larger PSII-LHCII absorptive cross section could reflect adaptation of the photosynthetic apparatus of *C*. sp. UWO241 to efficiently harvest energy under a natural light environmental of extreme shade and blue-green wavelengths (Morgan et al. 1998). This hypothesis was further supported by the observation that *C*. sp. UWO241 requires short wavelengths for growth and does not grown in red light (Morgan-Kiss et al. 2005). Conversely, this explanation does not extend to the psychrophilic *C*. sp. ICE-MDV which exhibits PSI-LHCI abundance and organization which is more comparable with the mesophilic *C. reinhardtii*.

While all three strains exhibited significant structural and functional changes to PSI, only minor effects on growth or photobiology in response to Fe-availability were observed. These data suggest that despite reductions the PSI/PSII ratio, all strains compensated their photochemistry to promote energy balance between PSII and PSI, as evidence by maintenance of high qP levels across all conditions (Fig. 2b). Photosynthetic organisms appear to compensate for reduced PSI under Fe-deficiency by increasing the effective cross section of PSI-LHCI. In Fe-starved cyanobacteria cells, there is an increase in the Chl *a* antenna protein, IsiA (Burnap et al. 1993; Michel and Pistorius 2004; Wilson et al. 2007; Chen et al. 2018), which forms an antenna ring around PSI trimers to make the PSI-IsiA supercomplex (Chen et al. 2018). A similar process occurs in the halophytic alga, *Dunaliella salina*, which accumulates a novel antenna protein, Tidi, under iron stress (Varsano et al. 2006). The Tidi protein is also associated with PSI-LHCI complexes. The Tidi-PSI-LHCI complexes migrated as large complexes on BN-PAGE and contained PsaA/B, PsaD as well as two Lhcas, p17.2 (Lhca2) and Lhca3 (Varsano et al. 2006). Lhca3 has also been implicated in acclimation to iron stress in *C. reinhardtii* (Naumann et al. 2005). During Fe-deprivation, PSI-LHCI supercomplexes accumulate as PSI particles which migrate at a lower sucrose density during sucrose density centrifugation and are associated with an N-terminally processed Lhca3 protein (Naumann et al. 2005). Interestingly, all of these examples of Fe-induced modifications to the LHCI antenna are associated with major changes in the 77 K fluorescence emission spectra including a loss of PSI fluorescence at ~712 nm and/or a shift in PSI-LHCI emission from red to blue wavelengths (Varsano et al. 2006; Naumann et al. 2005). These changes in PSI Chl *a* fluorescence were proposed to reflect either a reduction in Lhca proteins associated with red fluorescence and/or impairment of energy transfer from PSI to LHCI. Thus, while we did not directly study LHCI composition in this report, the loss of PSI-LHCI 77 K fluorescence emission in all three strains fits well with modification of PSI-LHCI organization across all three strains when grown under Fe-deficient conditions. Moreover, since Lhca3 is one of the few LHCI proteins detectable in *C*. sp. UWO241, this protein may play a significant role in the constitutive reorganization of PSI-LHCI in this strain. Alterations in the banding patterns of *C*. sp. UWO241 chlorophyll–protein complexes in sucrose gradients support also support the hypothesis that PSI-LHCI is reorganized under variable Fe availability (Fig. 8S).

P700 re-reduction kinetics showed that *C*. spp. UWO241 and ICE-MDV share a common phenotype of constitutively high rates of PSI-driven CEF which were maximal under

Fe-deficient conditions (Fig. 6b). This is in agreement with earlier reports of a strong capacity for CEF in *C*. sp. UWO241 (Morgan-Kiss et al. 2002b; Szyszka et al. 2007). CEF plays an important role in plants and algae, generating additional transthylakoid proton motive force (Munekage et al. 2004). The additional proton motive force can be used either to generate extra ATP to relieve imbalances in the ATP/NADPH ratio (Lucker and Kramer 2013) or to increase lumen pH for photoprotection of PSII by activating energy-dependent quenching (Yamori et al. 2016). In most plants and algae, CEF appears to be a minor process under nonstress conditions (Kramer and Evans 2011) and is maximally induced during periods of short-term environmental stress (Finazzi et al. 2002; Kono et al. 2014). In contrast, our results show that under steady-state growth conditions, both psychrophiles maintain constitutively high rates of CEF, regardless of growth conditions. While the mechanism of sustained CEF in the psychrophiles is not fully described, CEF in *C*. sp. UWO241 is associated with formation of a PSI supercomplex (Morgan-Kiss et al. 2005; Szyszka-Mroz et al. 2015). The physiological significance of sustained CEF remains to be fully defined. Higher steady-state levels of NPQ in the ELB isolates (Fig. 2d) suggest that CEF in the photopsychrophiles may play a role in providing constitutive photoprotection. Alternatively, there is significant evidence that growth under permanent low temperatures requires higher levels of ATP (Napolitano and Shain 2004). Last, CEF can prevent irreversible PSI photo-damage under environmental conditions (high salinity, low temperatures, fluctuating light) which promote over-reduction of PSI electron acceptors (Ivanov et al. 1998; Yamori et al. 2016; Huang et al. 2012). *C*. sp. UWO241 may possess additional mechanisms for protection of PSI, such as multiple isoforms of ferredoxin which possess different thermal properties (Cvetkovska et al. 2018).

Is the novel PSI phenotype of *C*. sp. UWO241 physiologically relevant? Reorganization of PSI demonstrates an important role in phytoplankton survival in low Fe-environments. The IsiA protein is highly expressed in high nutrient low chlorophyll (HNLC) habitats, where phytoplankton productivity is limited by Fe levels (Chen et al. 2018). Moreover, the effect of Fe on the adaptive strategy utilized by native phytoplankton populations is impacted by nutrient availability. In oligotrophic, low Fe conditions, IsiA is functionally attached to PSI, while under conditions of Fe-stress and nutrient replete conditions (a condition which mimics HNLC conditions), a large population of IsiA is functional detached from PSI (Behrenfeld et al. 2006; Schrader et al. 2011).

There are additional links between iron homeostasis and environmental stress. A recent proteomic study on a salt tolerant mutant of *C. reinhardtii* reported that relative the wild type strain, the mutant exhibited high expression of proteins associated with iron uptake and metabolism (Sithtisarn et al. 2017). *C*. sp. UWO241 is adapted to a hypersaline environment (> 700 mM) (Neale and Priscu 1990, 1995). It has been proposed that long-term adaptation to high salinity has dramatically altered the photosynthetic apparatus of this psychrophile (Dolhi et al. 2013; Szyszka-Mroz et al. 2015). Given the differential impact of iron on *C*. sp. UWO241 reported here, the high salinity environment could impact iron homeostasis. High salinity may interfere with iron uptake in *C*. sp. UWO241, resulting in permanent reorganization and/or downregulation of PSI as an adaptive strategy to chronic Fe-stress.

Based on our physiological and proteomic results of this study, we propose a model of restructuring of the photosynthetic apparatus of *C*. sp. UWO241 in response to variable iron (Fig. 10). Under standard growth conditions (18 µM Fe^{2+}), the photosynthetic apparatus is organized to support relatively high rates of PSI-mediated CEF. CEF-generated transthylakoid pmf produces ΔpH and membrane potential (Δψ) (Shikanai and Yamamoto 2017). A bestrophin-like protein dissipates Δψ through Cl^- influx into the lumen (Fig. 10a), allowing for maintenance of high transthylakoid ΔpH (Duan et al. 2016). CEF-generated ΔpH supports generation of NPQ, downregulating PSII. In addition, altered photosynthetic energy production in favor of ATP production may support rewired carbon metabolism, favoring carbon storage products (starch) and production of secondary stress metabolites through shikimate biosynthesis. When higher Fe levels are available, LEF is restored (although CEF remains relatively high) and fixed carbon is directed toward growth and biosynthesis (Fig. 10b).

In their native environment, the natural total iron levels of *C*. spp. UWO241 and ICE-MDV range within the Fe-deficient concentrations noted in other lakes (Morton and Lee 1974; Pollingher et al. 1995). Natural phytoplankton populations residing in the chemocline of ELB exhibit a 77 K fluorescence emission spectrum which closely resembles that of *C*. sp. UWO241 (i.e., low PSI Chl *a* fluorescence) (Kong et al. 2014). When incubated in filtered water collected from the same depth, both *C*. spp. UWO241 and ICE-MDV also exhibit comparable 77 K emission spectra with little to no PSI fluorescence (Fig. 9S). Thus, it is likely that reorganization of the PSI–LHCI complex is an important adaptation in the ELB phytoplankton populations to survive permanent low iron. Our results indicate that in its habitat of relatively freshwater and oligotrophic conditions at the surface of ELB, *C*. sp. ICE-MDV exhibits physiological plasticity and the ability to modulate its photosynthetic apparatus in response to environmental changes. Conversely, *C*. sp. UWO241 is a specialist, adapted to the deep photic zone where levels of macronutrients are sufficient, but hypersalinity is likely to play a significant role in the dramatic reorganization of the photosynthetic apparatus of this organism.

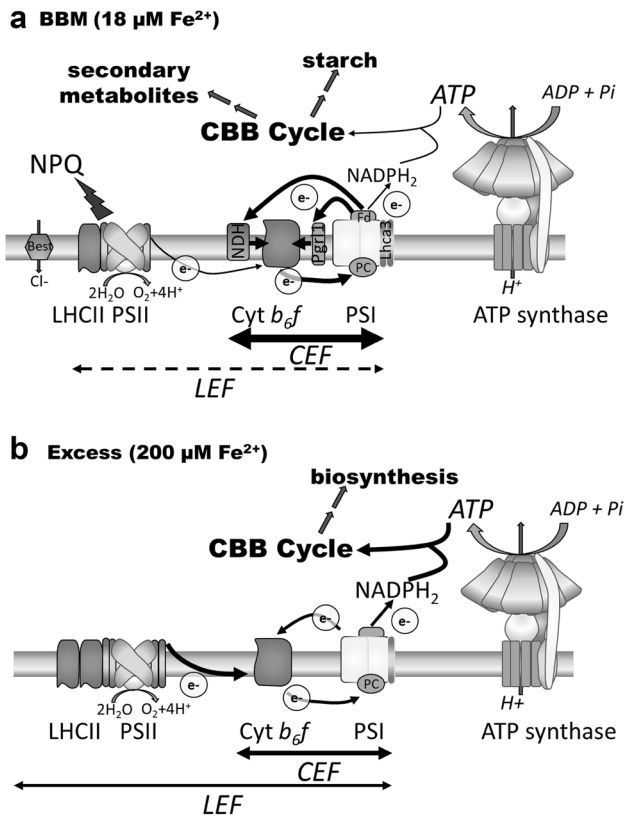

Fig. 10 Conceptual model of the impact of iron availability on the organization of the photosynthetic apparatus and downstream carbon metabolism in *C.* sp. UWO241. When grown in standard conditions (18 µM Fe^{2+}) (**a**), photosynthetic electron transport via linear electron flow (LEF) is downregulated, while enhanced rates of PSI-associated cyclic electron flow (CEF) generate high transthylakoid proton motive force (pmf). Dissipation of CEF-generated electric field gradient ($\Delta\Psi$) through a putative bestrophin (BEST)-like Cl^- channel may assist in maintenance of high transthylakoid ΔpH for induction of NPQ (Duan et al. 2016). Fixed carbon is stored as starch and secondary stress metabolites. Under excess Fe levels (200 µM Fe^{2+}) (**b**), photosynthetic electron transport is balanced between LEF and CEF. NPQ is minimal and fixed carbon is utilized for biosynthesis and growth

Acknowledgements The authors thank Prof. Joshua S. Yuan at Texas A&M University for helping us obtain the preliminary proteomics data for *C.* sp. UWO241.

Funding GC, IK, AT, WL, XW and RM-K were supported by NSF Grants OPP-1056396 and -1637708, DOE Grant DE-SC0019138. JP was supported by NSF Grant PLR-1637708.

Compliance with ethical standards

Conflict of interest The authors declare that they have no conflicts of interest.

References

Angino EE, Armitage KB, Tash JC (1964) Physicochemical limnology of Lake Bonney, Antarctica. Limnol Oceanogr 9(2):207–217

Armitage KB, House HB (1962) A limnological reconnaissance in the area of McMurdo Sound, Antarctica. Limnol Oceanogr 7(1):36–41

Asada K, Heber U, Schreiber U (1992) Pool size of electrons that can be donated to P700 + as determined in intact leaves: donation to P700 + from stromal components via the intersystem chain. Plant Cell Physiol 33(7):927–932

Behrenfeld MJ, Kolber ZS (1999) Widespread iron limitation of phytoplankton in the South Pacific Ocean. Science 283(5403):840–843

Behrenfeld MJ, Bale AJ, Kolber ZS, Aiken J, Falkowski PG (1996) Confirmation of iron limitation of phytoplankton photosynthesis in the equatorial Pacific Ocean. Nature 383(6600):508

Behrenfeld MJ, Worthington K, Sherrell RM, Chavez FP, Strutton P, McPhaden M, Shea DM (2006) Controls on tropical Pacific Ocean productivity revealed through nutrient stress diagnostics. Nature 442(7106):1025

Bibby TS, Nield J, Barber J (2001) Iron deficiency induces the formation of an antenna ring around trimeric photosystem I in cyanobacteria. Nature 412(6848):743

Bielewicz S, Bell EM, Kong W, Friedberg I, Priscu JC, Morgan-Kiss RM (2011) Protist diversity in a permanently ice-covered Antarctic lake during the polar night transition. ISME J 5:1559–1564

Bold HC (1949) The morphology of *Chlamydomonas chlamydogama* sp. nov. Bull Torrey Bot Club 76:101–108

Bowie AR, Whitworth DJ, Achterberg EP, Mantoura RFC, Worsfold PJ (2002) Biogeochemistry of Fe and other trace elements (Al, Co, Ni) in the upper Atlantic Ocean. Deep Sea Res Part I 49(4):605–636

Boyd PW, Watson AJ, Law CS, Abraham ER, Trull T, Murdoch R, Bakker DC, Bowie AR, Buesseler K, Chang H (2000) A mesoscale phytoplankton bloom in the polar Southern Ocean stimulated by iron fertilization. Nature 407(6805):695

Burnap RL, Troyan T, Sherman LA (1993) The highly abundant chlorophyll-protein complex of iron-deficient *Synechococcus* sp. PCC7942 (CP43′) is encoded by the *isiA* gene. Plant Physiol 103(3):893–902

Carvalho PC, Fischer JS, Chen EI, Yates JR, Barbosa VC (2008) PatternLab for proteomics: a tool for differential shotgun proteomics. BMC Bioinform 9(1):316

Chen H-Y, Bandyopadhyay A, Pakrasi H (2018) Function, regulation and distribution of IsiA, a membrane-bound chlorophyll a-antenna protein in cyanobacteria. Photosynthetica 56:322–333

Coale KH, Johnson KS, Chavez FP, Buesseler KO, Barber RT, Brzezinski MA, Cochlan WP, Millero FJ, Falkowski PG, Bauer JE (2004) Southern Ocean iron enrichment experiment: carbon cycling in high-and low-Si waters. Science 304(5669):408–414

Cvetkovska M, Hüner NP, Smith DR (2017) Chilling out: the evolution and diversification of psychrophilic algae with a focus on Chlamydomonadales. Polar Biol 40:1169–1184

Cvetkovska M, Szyszka-Mroz B, Possmayer M, Pittock P, Lajoie G, Smith DR, Hüner NP (2018) Characterization of photosynthetic ferredoxin from the Antarctic alga *Chlamydomonas* sp. UWO 241 reveals novel features of cold adaptation. New Phytol 219:588–604

De Baar HJ, De Jong JT, Bakker DC, Löscher BM, Veth C, Bathmann U, Smetacek V (1995) Importance of iron for plankton blooms and carbon dioxide drawdown in the Southern Ocean. Nature 373(6513):412

De Maayer P, Anderson D, Cary C, Cowan DA (2014) Some like it cold: understanding the survival strategies of psychrophiles. EMBO Rep 15(15):508–517

Desquilbet TE, Duval J-C, Robert B, Houmard J, Thomas JC (2003) In the unicellular red alga *Rhodella violacea* iron deficiency induces an accumulation of uncoupled LHC. Plant Cell Physiol 44(11):1141–1151

Dolhi JM, Maxwell D, Morgan-Kiss RM (2013) The Antarctic *Chlamydomonas raudensis*: an emerging model for cold adaptation of photosynthesis. Extremophiles 17:711–722

Dolhi JM, Teufel AG, Kong W, Morgan-Kiss RM (2015) Diversity and spatial distribution of autotrophic communities within and between ice-covered Antarctic lakes (McMurdo Dry Valleys). Limnol Oceanogr 60:977–991

Dore JE, Priscu JC (2001) Phytoplankton phosphorus deficiency and alkaline phosphatase activity in the McMurdo Dry Valley lakes, Antarctica. Limnol Oceanogr 46(6):1331–1346

Drop B, Webber-Birungi M, Fusetti F, Kouřil R, Redding KE, Boekema EJ, Croce R (2011) Photosystem I of *Chlamydomonas reinhardtii* contains nine light-harvesting complexes (Lhca) located on one side of the core. J Biol Chem 286(52):44878–44887

Duan Z, Kong F, Zhang L, Li W, Zhang J, Peng L (2016) A bestrophin-like protein modulates the proton motive force across the thylakoid membrane in Arabidopsis. J Integr Plant Biol 58(10):848–858

Elkhouni A, Rabhi M, Ivanov AG, Krol M, Zorrig W, Smaoui A, Abdelly C, Huner N (2018) Structural and functional integrity of *Sulla carnosa* photosynthetic apparatus under iron deficiency conditions. Plant Biol 20:415–425

Finazzi G, Rappaport F, Furia A, Fleischmann M, Rochaix JD, Zito F, Forti G (2002) Involvement of state transitions in the switch between linear and cyclic electron flow in *Chlamydomonas reinhardtii*. EMBO Rep 3(3):280–285

Frost B, Franzen N (1992) Grazing and iron limitation in the control of phytoplankton stock and nutrient concentration: a chemostat analogue of the Pacific equatorial upwelling zone. Mar Ecol Prog Ser 83(2):291–303

Glaesener AG, Merchant SS, Blaby-Haas CE (2013) Iron economy in *Chlamydomonas reinhardtii*. Front Plant Sci 4:337

Huang W, Yang S-J, Zhang S-B, Zhang J-L, Cao K-F (2012) Cyclic electron flow plays an important role in photoprotection for the resurrection plant *Paraboea rufescens* under drought stress. Planta 235(4):819–828

Ivanov AG, Morgan RM, Gray GR, Velitchkova MY, Huner NP (1998) Temperature/light dependent development of selective resistance to photoinhibition of photosystem I. FEBS Lett 430(3):288–292

Ivanov AG, Park YI, Miskiewicz E, Raven JA, Huner NP, Oquist G (2000) Iron stress restricts photosynthetic intersystem electron transport in *Synechococcus* sp. PCC 7942. FEBS Lett 485(2–3):173–177

Ivanov A, Sane P, Simidjiev I, Park Y-I, Huner N, Öquist G (2012) Restricted capacity for PSI-dependent cyclic electron flow in ΔpetE mutant compromises the ability for acclimation to iron stress in *Synechococcus* sp. PCC 7942 cells. Biochim Biophys Acta 1817(8):1277–1284

Jeffrey SW, Humphrey GF (1975) New spectrophotometric equations for determining chlorophyll a, b, c1, c2 in higher plants, algae and natural phytoplankton. Biochem Physiol Pflanz 167:191–194

Kong W, Ream DC, Priscu JC, Morgan-Kiss RM (2012) Diversity and expression of RubisCO genes in a perennially ice-covered Antarctic lake during the polar night transition. App Env Microbiol 78(12):4358–4366

Kong W, Li W, Prášil O, Romancova I, Morgan-Kiss RM (2014) An integrated study of photochemical function and expression of a key photochemical gene (*psbA*) in photosynthetic communities of Lake Bonney (McMurdo Dry Valleys, Antarctica). FEMS Microbiol Ecol 89(2):293–302

Kono M, Noguchi K, Terashima I (2014) Roles of the cyclic electron flow around PSI (CEF-PSI) and O_2-dependent alternative pathways in regulation of the photosynthetic electron flow in short-term fluctuating light in *Arabidopsis thaliana*. Plant Cell Physiol 55(5):990–1004

Kramer DM, Evans JR (2011) The importance of energy balance in improving photosynthetic productivity. Plant Physiol 155(1):70–78

Krause GH, Weis E (1991) Chlorophyll fluorescence and photosynthesis: the basics. Ann Rev Physiol Plant Mol Biol 42:313–349

Kumar S, Stecher G, Tamura K (2016) MEGA7: molecular evolutionary genetics analysis version 7.0 for bigger datasets. Mol Biol Evol 33(7):1870–1874

La Rocca N, Sciuto K, Meneghesso A, Moro I, Rascio N, Morosinotto T (2015) Photosynthesis in extreme environments: responses to different light regimes in the Antarctic alga Koliella antarctica. Physiol Plant 153(4):654–667

Li W, Podar M, Morgan-Kiss RM (2016) Ultrastructural and single-cell-level characterization reveals metabolic versatility in a microbial eukaryote community from an Ice-covered Antarctic Lake. Appl Environ Microbiol 82(12):3659–3670

Lucker B, Kramer DM (2013) Regulation of cyclic electron flow in *Chlamydomonas reinhardtii* under fluctuating carbon availability. Photosynth Res 117(1–3):449–459

Lukeš M, Procházková L, Shmidt V, Nedbalová L, Kaftan D (2014) Temperature dependence of photosynthesis and thylakoid lipid composition in the red snow alga Chlamydomonas cf. nivalis (Chlorophyceae). Fems Microbiol Ecol 89(2):303–315

Lyons WB, Fountain AG, Doran PT, Priscu J, Neumann K (2000) The importance of landscape position and legacy: the evolution of the Taylor Valley Lake District. Freshwat Biol 43:355–367

Martin JH (1990) Glacial-interglacial CO_2 change: the iron hypothesis. Paleoceanogr 5(1):1–13

Martin JH (1992) Iron as a limiting factor in oceanic productivity. In: Primary productivity and biogeochemical cycles in the sea. Springer, New York, pp 123–137

Martin JH, Fitzwater SE (1988) Iron deficiency limits phytoplankton growth in the north-east Pacific subarctic. Nature 331(6154):341

Merchant SS, Allen MD, Kropat J, Moseley JL, Long JC, Tottey S, Terauchi AM (2006) Between a rock and a hard place: trace element nutrition in *Chlamydomonas*. Biochim Biophys Acta 1763(7):578–594

Michel KP, Pistorius EK (2004) Adaptation of the photosynthetic electron transport chain in cyanobacteria to iron deficiency: the function of IdiA and IsiA. Physiol Plant 120(1):36–50

Mock T, Otillar RP, Strauss J, McMullan M, Paajanen P, Schmutz J, Salamov A, Sanges R, Toseland A, Ward BJ (2017) Evolutionary genomics of the cold-adapted diatom *Fragilariopsis cylindrus*. Nature 541(7638):536

Molot LA, Dillon PJ (2003) Variation in iron, aluminum and dissolved organic carbon mass transfer coefficients in lakes. Water Res 37(8):1759–1768

Morgan RM, Ivanov AG, Priscu JC, Maxwell DP, Hüner NPA (1998) Structure and composition of the photochemical apparatus of the Antarctic green alga, *Chlamydomonas subcaudata*. Photosyn Res 56:303–314

Morgan-Kiss R, Ivanov AG, Williams J, Mobashsher K, Hüner NP (2002a) Differential thermal effects on the energy distribution between photosystem II and photosystem I in thylakoid membranes of a psychrophilic and a mesophilic alga. Biochim Biophys Acta 1561(2):251–265

Morgan-Kiss RM, Ivanov AG, Hüner NPA (2002b) The Antarctic psychrophile, *Chlamydomonas subcaudata*, is deficient in state I-state II transitions. Planta 214(3):435–445

Morgan-Kiss RM, Ivanov AG, Pocock T, Król M, Gudynaite-Savitch L, Hüner NPA (2005) The Antarctic psychrophile, *Chlamydomonas raudensis* Ettl (UWO241) (CHLOROPHYCEAE, CHLOROPHYTA) exhibits a limited capacity to photoacclimate to red light. J Phycol 41:791–800

Morgan-Kiss RM, Priscu JC, Pocock T, Gudynaite-Savitch L, Huner NP (2006) Adaptation and acclimation of photosynthetic microorganisms to permanently cold environments. Microbiol Mol Biol Rev 70(1):222–252

Morgan-Kiss RM, Ivanov A, Modla S, Cyzmmek K, Huner NPA, Priscu JC, Hanson TE (2008) Identity and phylogeny of a new psychrophillic eukaryotic green alga, *Chlorella* sp. strain BI isolated from a transitory pond near Bratina Island. Antarctica Extremophiles 12:701–711

Morton SD, Lee TH (1974) Algal blooms. Possible effects of iron. Environ Sci Technol 8(7):673–674

Moseley JL, Allinger T, Herzog S, Hoerth P, Wehinger E, Merchant S, Hippler M (2002) Adaptation to Fe-deficiency requires remodeling of the photosynthetic apparatus. EMBO J 21(24):6709–6720

Munekage Y, Hashimoto M, Miyake C, Tomizawa K-I, Endo T, Tasaka M, Shikanai T (2004) Cyclic electron flow around photosystem I is essential for photosynthesis. Nature 429(6991):579–582

Napolitano MJ, Shain DH (2004) Four kingdoms on glacier ice: convergent energetic processes boost energy levels as temperatures fall. Proc R Soc Lond B 271:273–276

Naumann B, Stauber EJ, Busch A, Sommer F, Hippler M (2005) N-terminal processing of Lhca3 is a key step in remodeling of the photosystem I-light-harvesting complex under iron deficiency in *Chlamydomonas reinhardtii*. J Biol Chem 280(21):20431–20441

Naumann B, Busch A, Allmer J, Ostendorf E, Zeller M, Kirchhoff H, Hippler M (2007) Comparative quantitative proteomics to investigate the remodeling of bioenergetic pathways under iron deficiency in *Chlamydomonas reinhardtii*. Proteomics 7(21):3964–3979

Neale PJ, Priscu JC (1990) Structure and function of the photochemical apparatus in the phytoplankton of ice-covered Lake Bonney. Antarc J US 25(5):225–225

Neale PJ, Priscu JC (1995) The photosynthetic apparatus of phytoplankton from a perennially ice-covered Antarctic lake: acclimation to an extreme shade environment. Plant Cell Physiol 36:253–263

Pfündel E, Klughammer C, Schreiber U (2008) Monitoring the effects of reduced PS II antenna size on quantum yields of photosystems I and II using the Dual-PAM-100 measuring system. PAMM App Notes 1:21–24

Pollingher U, Kaplan B, Berman T (1995) The impact of iron and chelators on Lake Kinneret phytoplankton. J Plank Res 17(10):1977–1992

Priscu JC (1995) Phytoplankton nutrient deficiency in lakes of the McMurdo Dry Valleys, Antarctica. Freshw Biol 34:215–227

Priscu JC, Wolf CF, Takacs CD, Fritsen CH, Laybourn-Parry J, Roberts JKM, Berry-Lyons W (1999) Carbon transformations in the water column of a perennially ice-covered Antarctic Lake. Biosci 49:997–1008

Ravenel J, Peltier G, Havaux M (1994) The cyclic electron pathways around photosystem I in *Chlamydomonas reinhardtii* as determined *in vivo* by photoacoustic measurements of energy storage. Planta 193:251–259

Raymond JA, Morgan-Kiss R (2013) Separate Origins of ice-binding proteins in Antarctic *Chlamydomonas* species. PLoS ONE 8(3):e59186

Raymond J, Morgan-Kiss RM (2017) Multiple ice-binding proteins of probably prokaryotic origin in an Antarctic lake alga, *Chlamydomonas* sp. ICE-MDV (Chlorophyceae). J Phycol 53(4):848–854

Schrader PS, Milligan AJ, Behrenfeld MJ (2011) Surplus photosynthetic antennae complexes underlie diagnostics of iron limitation in a cyanobacterium. PLoS ONE 6(4):e18753

Shaked Y, Erel Y, Sukenik A (2004) The biogeochemical cycle of iron and associated elements in Lake Kinneret1, 2. Geochim Cosmochim Acta 68(7):1439–1451

Shikanai T, Yamamoto H (2017) Contribution of cyclic and pseudocyclic electron transport to the formation of proton motive force in chloroplasts. Mol Plant 10(1):20–29

Siththisarn S, Yokthongwattana K, Mahong B, Roytrakul S, Paemanee A, Phaonakrop N, Yokthongwattana C (2017) Comparative proteomic analysis of *Chlamydomonas reinhardtii* control and a salinity-tolerant strain revealed a differential protein expression pattern. Planta 246(5):843–856

Sonoike K, Terashima I (1994) Mechanism of photosystem-I photoinhibition in leaves of *Cucumis sativus* L. Planta 194:287–293

Sonoike K, Terashima I, Iwaki M, Itoh S (1995) Destruction of photosystem I iron-sulfur centers in leaves of *Cucumis sativus* L. by weak illumination at chilling temperatures. FEBS Lett 362(2):235–238

Spigel RH, Priscu JC (1998) Physical limnology of the McMurdo Dry Valley lakes. In: Priscu JC (ed) Ecosystem dynamics in a polar desert: the McMurdo dry valleys, Antarctica. Antarctic Research Series, vol 72. American Geophysical Union, pp 153–187

Spreitzer RJ, Mets L (1981) Photosynthesis-deficient mutants of *Chlamydomonas reinhardii* with associated light-sensitive phenotypes. Plant Physiol 67(3):565–569

Stauber EJ, Busch A, Naumann B, Svatoš A, Hippler M (2009) Proteotypic profiling of LHCI from *Chlamydomonas reinhardtii* provides new insights into structure and function of the complex. Proteomics 9(2):398–408

Straus NA (1994) Iron deprivation: physiology and gene regulation. In: The molecular biology of cyanobacteria. Springer, New York, pp 731–750

Strzepek RF, Harrison PJ (2004) Photosynthetic architecture differs in coastal and oceanic diatoms. Nature 431(7009):689

Szyszka B, Ivanov AG, Huner NPA (2007) Psychrophily induces differential energy partitioning, photosystem stoichiometry and polypeptide phosphorylation in *Chlamydomonas raudensis*. Biochim Biophys Acta 1767:789–800

Szyszka-Mroz B, Pittock P, Ivanov AG, Lajoie G, Hüner NP (2015) The Antarctic psychrophile, *Chlamydomonas* sp. UWO 241, preferentially phosphorylates a PSI-cytochrome b6/f supercomplex. Plant Physiol 169:717–736

Tamura K, Nei M, Kumar S (2004) Prospects for inferring very large phylogenies by using the neighbour-joining method. Proc Nat Acad Sci USA 101:11030–11035

Teufel AG, Li W, Kiss AJ, Morgan-Kiss RM (2017) Impact of nitrogen and phosphorus on phytoplankton production and bacterial community structure in two stratified Antarctic lakes: a bioassay approach. Polar Biol 40(5):1007–1022

Varsano T, Wolf SG, Pick U (2006) A chlorophyll a/b-binding protein homolog that is induced by iron deficiency is associated with enlarged photosystem I units in the eucaryotic alga *Dunaliella salina*. J Biol Chem 281(15):10305–10315

Vizcaíno JA, Csordas A, Del-Toro N, Dianes JA, Griss J, Lavidas I, Mayer G, Perez-Riverol Y, Reisinger F, Ternent T (2015) 2016 update of the PRIDE database and its related tools. Nucl Acids Res 44(D1):D447–D456

Wang X, Liu W, Xin C, Zheng Y, Cheng Y, Sun S, Li R, Zhu X-G, Dai SY, Rentzepis PM (2016) Enhanced limonene production in cyanobacteria reveals photosynthesis limitations. Proc Natl Acad Sci USA 113(50):14225–14230

Ward BB, Granger J, Maldonado MT, Wells MR (2003) What limits bacterial production in the suboxic region of permanently ice-covered Lake Bonney, Antarctica. Aquat Microbial Ecol 31:33–47

Weand BL, Hoehn RC, Parker BC (1976) Trace element distributions in an Antarctic meromictic lake. Aquat Ecol 10(2):104–114

Wilson A, Boulay C, Wilde A, Kerfeld CA, Kirilovsky D (2007) Light-induced energy dissipation in iron-starved cyanobacteria: roles of OCP and IsiA proteins. Plant Cell 19(2):656–672

Xu T, Venable J, Park SK, Cociorva D, Lu B, Liao L, Wohlschlegel J, Hewel J, Yates III J (2006) ProLuCID, a fast and sensitive tandem mass spectra-based protein identification program. In: Molecular & cellular proteomics, vol 10. Amer Soc Biochemistry Molecular Biology Inc, p S174

Yadavalli V, Jolley CC, Malleda C, Thangaraj B, Fromme P, Subramanyam R (2012) Alteration of proteins and pigments influence the function of photosystem I under iron deficiency from *Chlamydomonas reinhardtii*. PLoS ONE 7(4):e35084

Yamori W, Makino A, Shikanai T (2016) A physiological role of cyclic electron transport around photosystem I in sustaining photosynthesis under fluctuating light in rice. Sci Rep 6:20147

Yi-Bin W, Fang-Ming L, Xiu-Fang Z, Ai-Jun Z, Bin W, Zhou Z, Cheng-Jun S, Jin-Lai M (2017) Composition and regulation of thylakoid membrane of Antarctic ice microalgae Chlamydomonas sp. ICE-L in response to low-temperature environment stress. J Mar Biol Assoc UK 97(6):1241–1249

Zhang Z, An M, Miao J, Gu Z, Liu C, Zhong B (2018) The Antarctic sea ice alga *Chlamydomonas* sp. ICE-L provides insights into adaptive patterns of chloroplast evolution. BMC Plant Biol 18(1):53